

Seventh Framework Programme

Theme 6

Environment



Project: 603864 – HELIX

Full project title:

High-End cLimate Impacts and eXtremes

Deliverable: 4.5

**Provision of impact simulations based on the new AGCM time
slice simulations for 3 SWLs**

Version 1.0

Original Due date of deliverable: 31/10/16

Actual date of submission: 31/01/17

**Provision of
impact
simulations
based on the
new AGCM
time slice
simulations
for 3 SWLs**

January

2017

Pierre Friedlingstein, Catherine Morfopoulos, Richard Betts, University of Exeter
Nicole Forstenhaeusler, Jeff Price, Rachel Warren, University of East Anglia
Gustavo Naumann, Lorenzo Alfieri, Luc Feyen, European Commission, Joint Research Centre
Ioannis K. Tsanis, Lamprini Papadimitriou, Aristeidis Koutroulis, Technical University of Crete

1. Introduction

This deliverable describes the future simulations performed with the HELIX impact models, in order to investigate impacts on different systems for Specific Warming Levels (SWL) of 1.5°C, 2°C and 4°C. The impact models used here represent crop yield, biodiversity, water resources, river floods and global droughts.

In general, the HELIX impact models were driven by high resolution (0.5°x0.5°) climate forcing from two climate models: EC-Earth and HadGEM3. Both models were driven by the RCP8.5 scenario (greenhouse gases forcing) as well as by prescribed sea surface temperature (SSTs) coming from a range of CMIP5 climate simulations as used in the 5th assessment of the Intergovernmental Panel on Climate Change (IPCC 2013), resulting in an ensemble of climate forcing datasets. A total of 9 members of the high resolution climate forcing ensemble were made available to the impact modelling groups. All climate forcing have been bias corrected using the Princeton Princeton v2 hybrid dataset of observed climate variables (temperature, precipitation, winds, surface pressure, radiation, etc) (Sheffield et al., 2006). For most impacts, a number of ensemble members were used to drive the impacts models, although some (crops and biomes) used a more limited set at this stage. For one impact, biodiversity, the above methodology was not used. Climate forcing was taken from the AVOID2 (Avoiding Dangerous Climate Change) project funded by the UK Department of Energy and Climate Change (Bernie & Lowe, 2014). This is because of the delay of provision of the HELIX climate forcing and the large computing time required for the biodiversity simulations (see section 3.2).

The time (calendar year) of reaching SWL of 1.5°C, 2°C and 4°C were diagnosed from the bias correct time series of global average surface temperature for each climate forcing (Table 1.1). Impact models used this information to select the 30-year time periods centred on SWL 1.5, SWL 2 and SWL 4 associated with each GCM. The use of different SSTs as boundary conditions of the hi-resolution atmospheric climate models allow to explore a larger range of climate sensitivities. For example, SWL of 2°C is reached in 2035 for EC-EARTH forced by the HadGEM2-ES SSTs, but only in 2054 with the GFDL-ESM2M SSTs.

Table 1.1 Time of reaching specific warming levels of 1.5, 2 and 4°C in each bias corrected forcing from the hi-resolution climate simulations, driven by different sets of CMIP5 sea surface temperatures.

Hi-Res. Climate Model	Driving SSTs	SWL:1.5	SWL:2.0	SWL:4.0
EC-EARTH R1	IPSL-CM5A-LR	2025	2036	2074
EC-EARTH R2	GFDL-ESM2M	2038	2054	n/a
EC-EARTH R3	HadGEM2-ES	2021	2035	2075
EC-EARTH R4	EC-EARTH	2028	2043	2090
EC-EARTH R5	GISS-E2-H	2031	2047	n/a
EC-EARTH R6	IPSL-CM5A-LR	2024	2038	2072
EC-EARTH R7	HadCM3LC	2026	2040	2088
HadGEM-R1	IPSL-CM5A-LR	2024	2035	2071
HadGEM-R3	HadGEM2-ES	2019	2033	2071

2. Crop Yield

2.1 Model Used and Brief Description

To investigate the impacts of differing levels of increase in global temperature on crop yield we developed statistical crop yield models (CropClim) based on historical crop yield and climate data using the machine learning technique Random Forests (RF).

Crop Yield data was obtained from the Food and Agriculture Organization of the United Nations (FAO). FAO collects data for a variety of food security related variables including a regularly updated set for crop production, area harvested and yield. We downloaded the complete set covering a total of 176 crops, crop combinations and food plants for up to 222 countries for the time period 1961-2013. The data was checked regarding suitability for regression analysis following the protocol of Zuur et al. (2010). We obtained crop calendar maps developed by Sacks et al. (2010) and used them to calculate maximum temperature and precipitation during the growing season of 19 crops for which the maps were available.

To develop the CropClim models and project future crop yield we developed RF models in R. Random Forests can be used for classification and regression and here we used them to regress crop yield on climate variables. We limited the number of climate variables to reduce issues of multicollinearity and to reduce the danger of 'overfitting' the climate variables using stepwise reduction. We used the natural logarithm of the yield as the response variable following Lobell et al. (2011).

In a previous study Lobell et al. (2008) developed time-series regression models for hunger importance (HI) regions to project crop yield or crop production (depending on crop). Instead of using a time-series approach we used the models to derive projections of the average crop yield per crop and country for a 30-year period. In most cases the spatial aggregation of yearly yield values increased the number of available observations per crop and allowed the inclusion of additional predictor variables apart from maximum temperature and precipitation during a crop's growing season. Depending on the number of countries planting a crop it was thus possible to develop models based on up to 6 variables. A further subdivision of the data to develop regional models as presented by Lobell et al. (2008) was not feasible due to the limited amount of observations. However, for each crop we developed up to six models based on different sets of predictors of which half incorporated the continent a country is located in as fixed factor. The best model for each crop was selected based on the minimum RSME achieved during repeated cross-validation (100 times, 10 folds).

2.2 Simulations performed

The climate variables used to train and test the models were obtained from CRU TS 3.22. Using the CRU observed data allowed us better comparability to previous statistical modelling exercises as they also used a version of the CRU observed data (Lobell et al. 2008). Values for the baseline period of 1980-2010 were used for training and cross-validation and subsequently each model was tested against the average values for the time period 1961-1990. We then ran the models on the output of

the high-resolution Helix models Hadgem3-r1 and EC-Earth-r1 selecting the 30-year time periods centred around SWL 1.5, SWL 2 and SWL 4 associated with each GCM.

Currently models for 70 crops (**CropClim**) have been developed and for 25 of them runs on both HadGEM and EC-Earth data have been completed for SWL 1.5, SWL 2 and SWL 4. Running the remaining models for the three SWLs is in progress and additional simulations out to 6°C are planned. Additional work will be undertaken to examine the role of fertilizer use as well as to look at adaptation options, including irrigation and the potential role of CO₂ fertilization. We will also look at population levels in these regions and how the changes in yields may impact human populations. Unlike many of the current physiologically based crop models, the **CropClim** approach autonomously allows for shifting crop ranges and timings, and rapidly allows the development of models for crops not usually examined in other studies (which typically look at the main 4-5 crops; the “big 4” being rice, maize, wheat and soybean). CropClim allows us to examine additional crops important in developing countries as well as allows us to look for key crops that may be needed to replace the “big 4” in some regions.

2.3 Results

The figures 2.1 to 2.4 below are a sample of the output obtained and display potential impacts on the yield of rice, wheat, maize and potatoes. It is estimated that the human population will grow to around 9 billion by 2050 and to satisfy the resulting demand the amount of food has to be considerably increased (Godfray et al., 2010). As free areas to convert for agricultural needs become increasingly rare, maximisation of yield and closure of existing yield gaps is of vital importance (Godfray et al., 2010) and the figures presented below give an indication about the impact on rice, maize, wheat and potato yield in different world regions that can be expected under 1.5°-4°C warming based on data from two different GCMs.

CropClim provides an importance ranking for the climate predictors the model is based on and dependency plots (not presented) allow an analysis of the effects of changes of each variable. It is thus possible to identify temperature and precipitation values for which crop yield becomes optimal or at least lead to a beneficial outcome. It also allows to subsequently analyse water availability or use of irrigation in potentially overcoming precipitation changes.

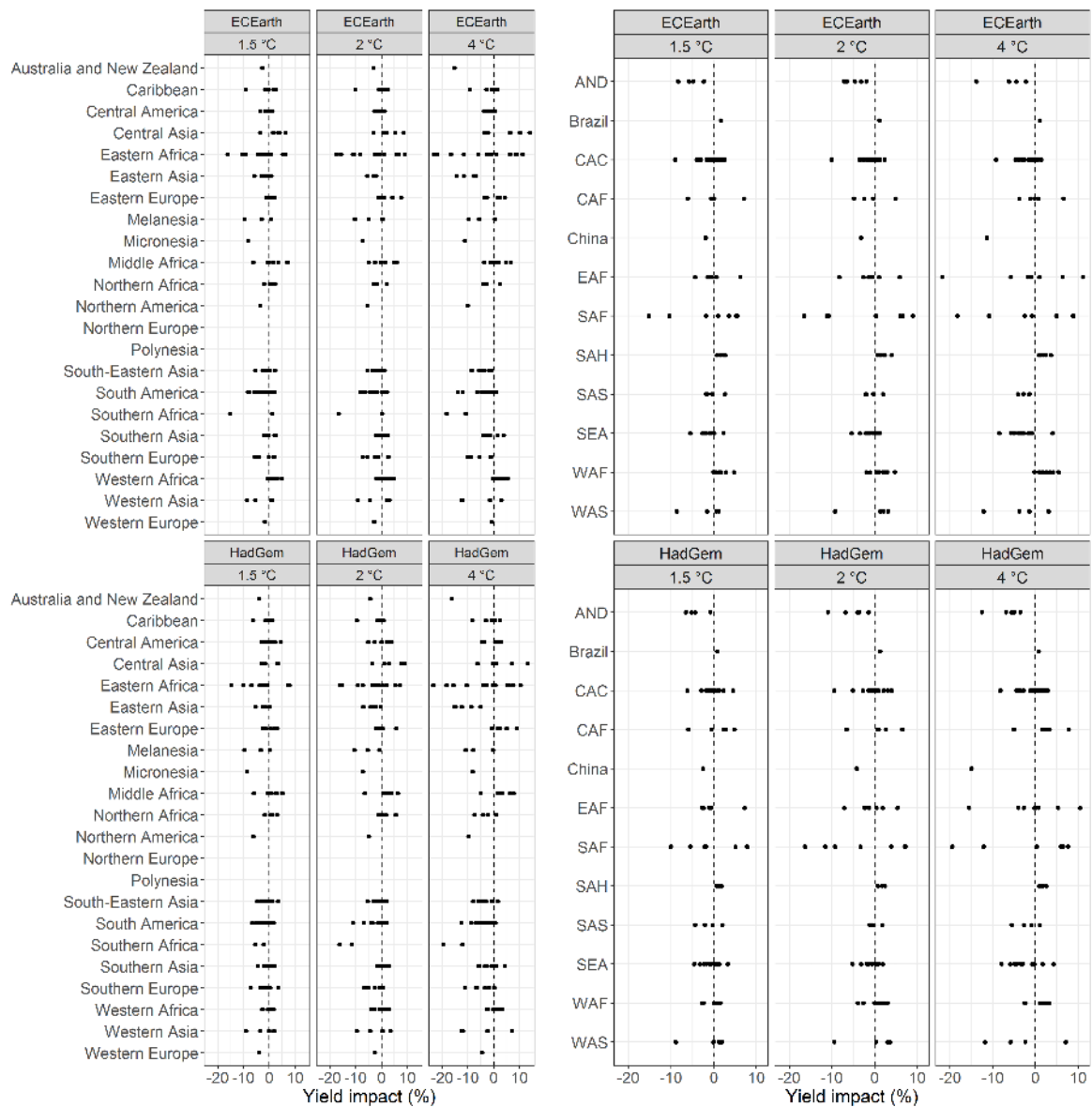


Figure 2.1. Potential impacts on average rice yield separated by GCM for 22 global regions and 12 HI regions as defined by Lobell et al. (2008). Regions in which no data point appears do not grow this crop.

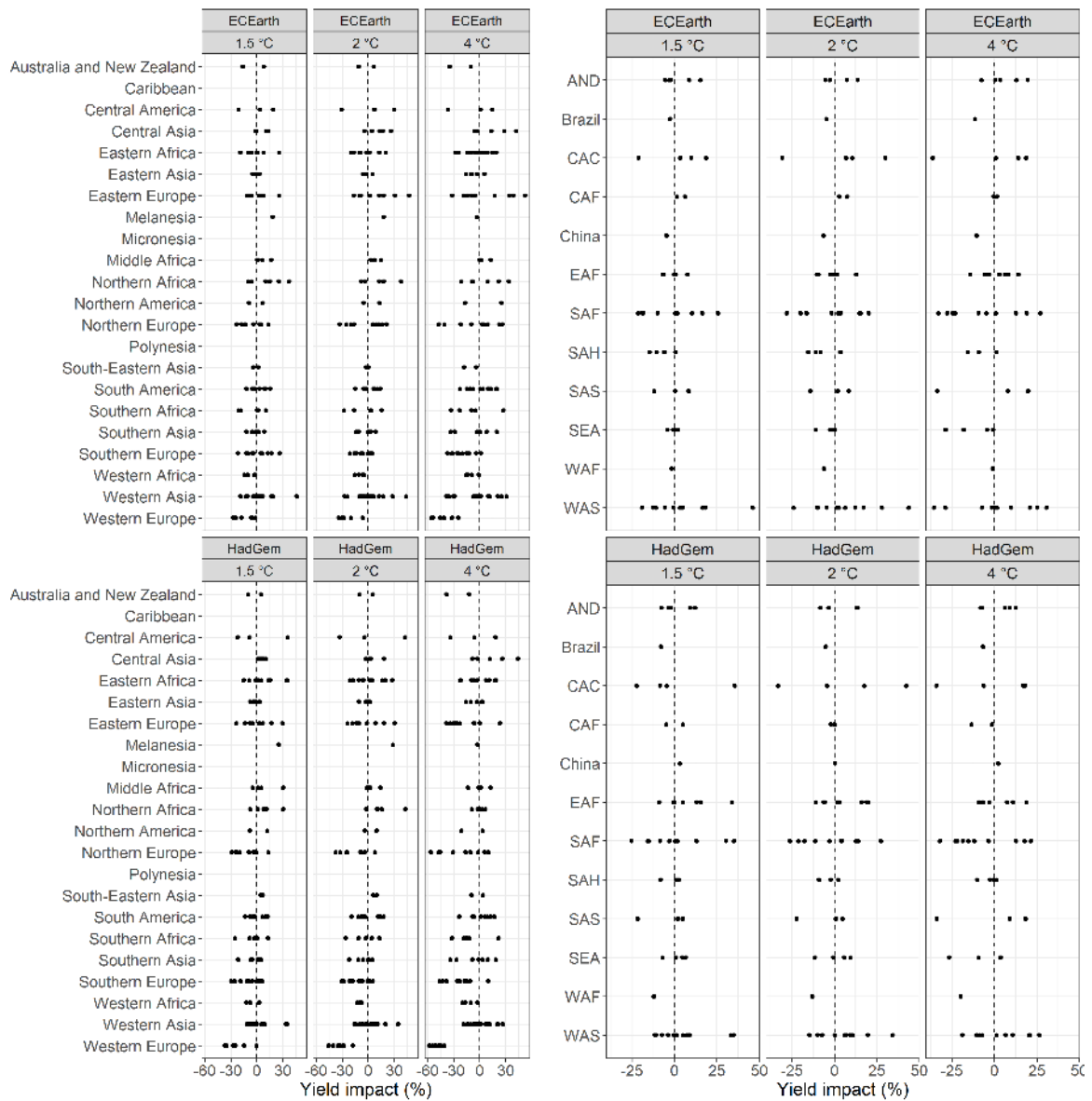


Figure 2.2. Potential impacts on average wheat yield separated by GCM for 22 global regions and 12 HI regions.

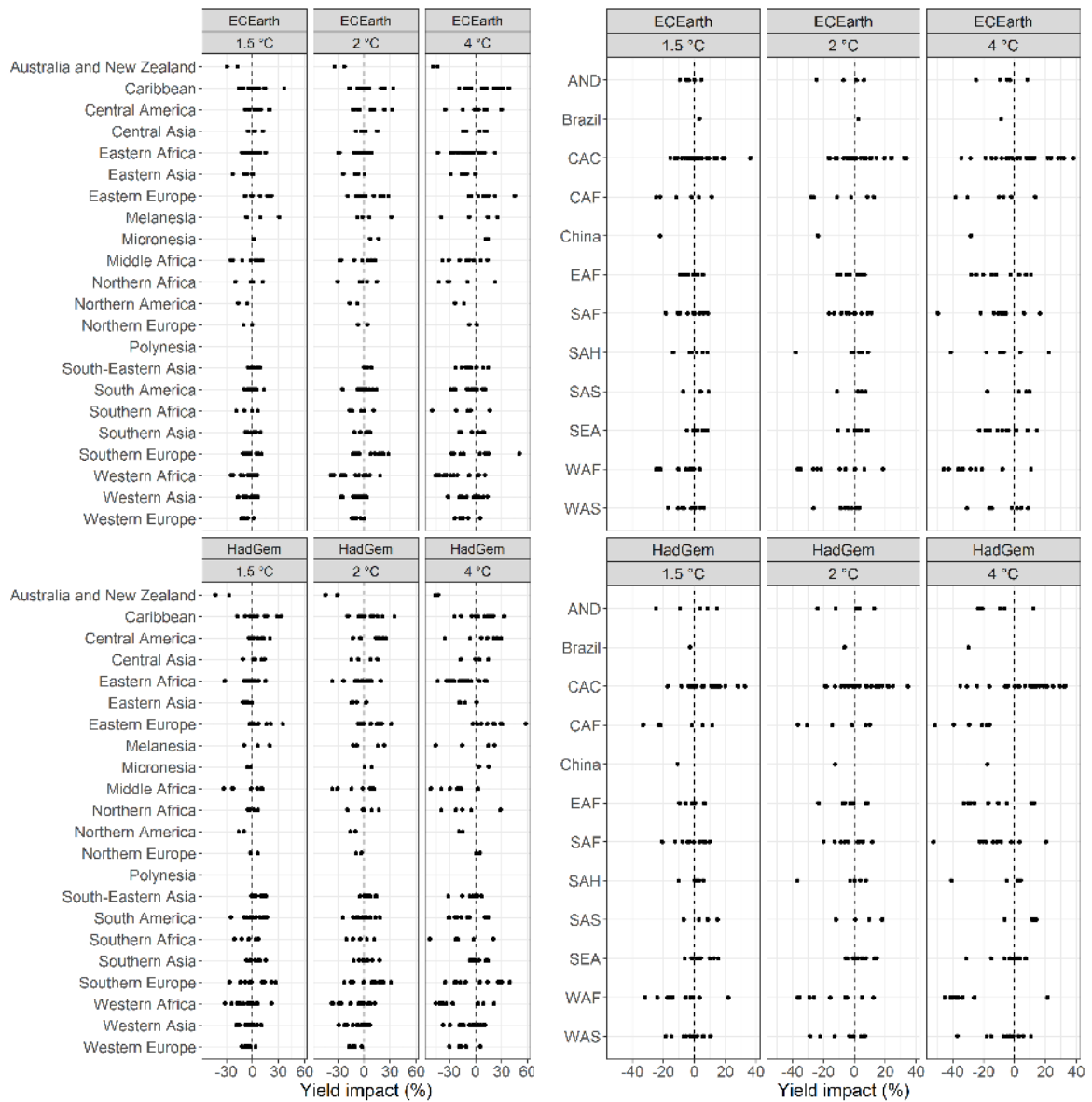


Figure 2.3. Potential impacts on average maize yield separated by GCM for 22 global regions and 12 HI regions.

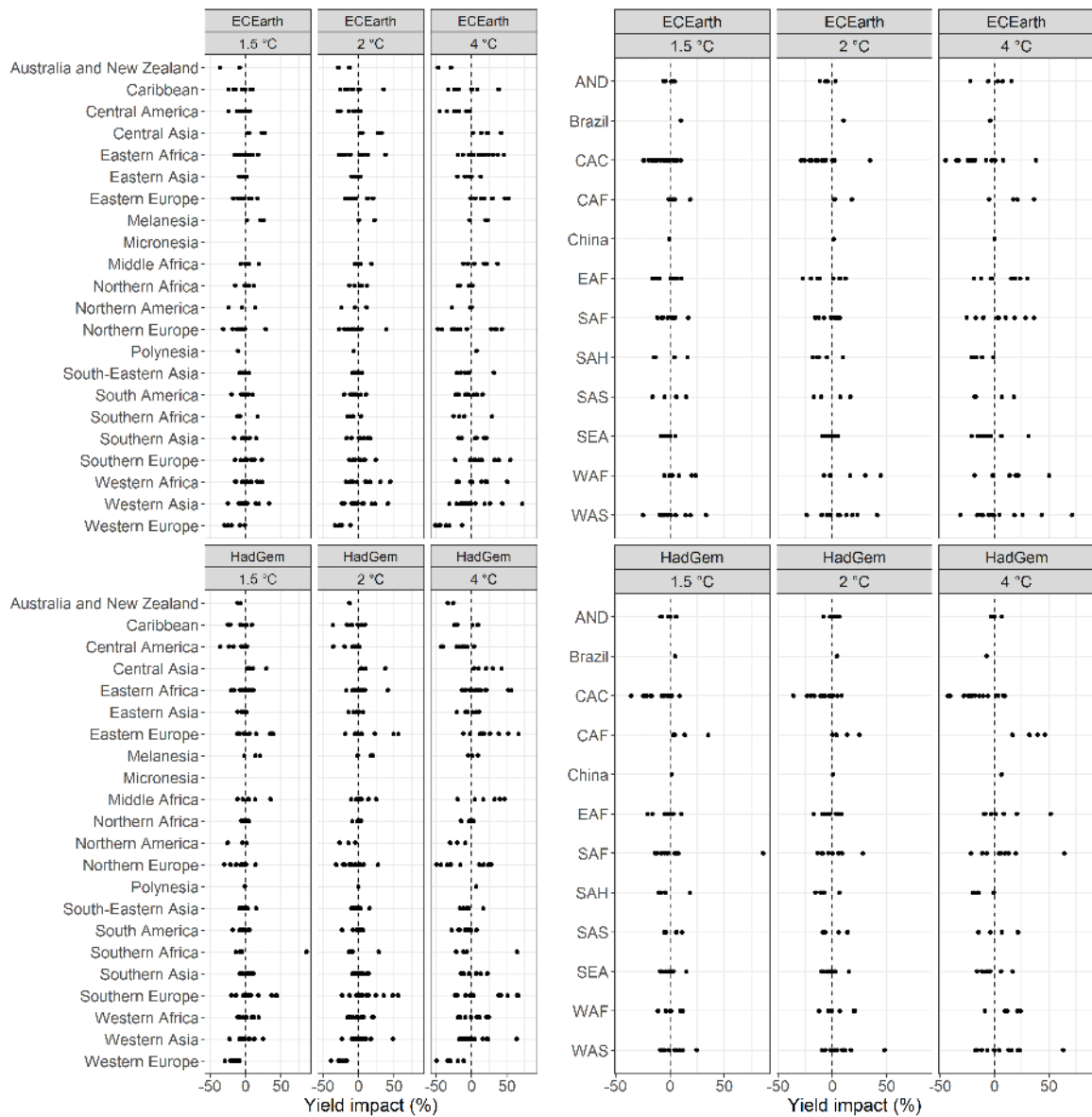


Figure 2.4. Potential impacts on average potato yield separated by GCM for 22 global regions and 12 HI regions.

2.4 Discussion

Figures 2.1 to 2.4 display the projected impacts based on both of the GCMs for 1.5°C, 2°C and 4°C of average global warming. Generally, the GCMs lead to similar projections with occurrences of high differences between them being moderate. On the global scale the projections suggest a decrease of yield for rice, maize and wheat and a stagnation of potato yield for SWL 4. Impacts on different regions display a much more varied picture and differences for countries within the same region can be considerably large.

Although a temperature variable associated with a decline of yield above a certain value was selected as the most important predictor for either of the four crops presented, an increase in global temperature does not necessarily result in decrease of yield within each country. Precipitation also plays an important role and potential interactions between them add to the complexity of the system.

The models give a useful indication based on the information they are given to operate on but there are many variables which have been omitted which could have an effect in either direction, positive and negative. For instance, we did not consider fertiliser input, a potential positive impact of elevated CO₂ or a shift to genetically improved crop species which can tolerate conditions which are considered unfavourable for the ones grown at present and in the past. On the other hand, the projections might be too optimistic as an increase of extreme weather events (e.g. droughts, floods, heatwaves and resulting fire regimes) is not incorporated. The mean values used in this study might well be in the range of those values which crop species already experience on a daily base thus leading only to a small decrease in average yield. A long drought or fire regime on the other hand is able to destroy the yield of a whole region and has thus a much higher impact.

However, all the projections are likely to be conservative, because statistical models, as compared to process-based models, are unable to extend predictions outside the range of already observed values without assuming linearity of the response. For regression trees this problem becomes even worse as their nature completely prohibits any extrapolation for values outside the training range. For a lower SWL this might not be a big issue but predictions for the end of the 21st century are more likely to be affected by this restriction. This will be examined further within this project.

3. Biodiversity

3.1 Brief description of impact model used

The impact model used for biodiversity is that used in the Wallace Initiative and previously published (Warren et al 2013). The basic approach is that species distribution data and climate observations are used to create trained climatic envelope models in MaxEnt (Elith et al. 2010) and projected climates are then used to simulate potential future climate space for each species, including or excluding the potential for species to move by dispersal to track climate change over the earth's surface. For this study we used newly developed models of ~80,000 plants, birds, mammals, reptiles and amphibians for multiple dispersal scenarios at a spatial resolution of 20km x 20km. The initial runs (described below) generated almost 1 petabyte of data and is the most thorough modelling exercise of its type for biodiversity to date.

Primary biodiversity distribution data were obtained from the Global Biodiversity Information Facility (GBIF). GBIF facilitates discovery of data from many datasets worldwide, including newer efforts such as eBird (Cornell Laboratory of Ornithology, ebird.org), which allows birdwatchers to enter their birding records. While there are still some gaps in the available data, GBIF provides a source allowing researchers to identify potential patterns of change across the widest range of species and areas possible. The data were then checked for locational consistency and outliers (Warren et al. 2013). Bioclimatic models were then developed using the program MaxEnt using a limited set of eight climate variables in order to minimize potential issues with autocorrelation and to prevent 'overfitting' of the MaxEnt modelled species distributions.

We used the projected climates and trained models to derive potential future climate space for each species in our future climate scenarios for SWLs of 1.5° (no dispersal only), 2°, 4° and 6° equating to 30-year periods centred on 2025, 2055 and 2085 in different emission scenarios. To each future projection, we applied two class-specific 'dispersal' scenarios (referring to the rates at which species' ranges shift over time, see below) as a buffer (distance defined by the rate of movement and the number of years into the future) around this current distribution, given a continuous land surface and allowing dispersal to contiguous land areas. In this study the dispersal rate refers to the average long-term shift of an entire species' range (taken from the published literature of current observed changes and paleoecological changes) taking into account potential repeated colonization and extinction events until a species' entire range catches up with the new 'environmental space'. Most previous studies of this kind only look at two dispersal scenarios – none and full. For this study we included a zero dispersal rate as one scenario, in common with many previous studies. However, contrary to many studies, we did not look at a "full" dispersal scenario, where species are allowed to instantly move into the new available climate space, as we do not feel this is a realistic representation of what actually occurs in nature. The typical dynamics of range shifts (through multiple dispersal, colonization, extirpation and rescue events), barriers to movements, lack of instant availability of suitable soils or habitats, as well as lack of a stabilized climate (within the timeframes of this study) are just some of the factors making a 'full' dispersal scenario unlikely within the timeframe of this study in the absence of assisted movement. Instead, we looked at a 'realistic' dispersal scenario per taxa, based on dispersal rates found in the literature. In these scenarios, we allow species to move to fill their new climate envelope at the rate specified, provided they do not move across sea or ocean barriers.

The dispersal rates chosen for this study come from a review of the literature (see Warren *et al.* 2013 for more details). Based on the literature we chose a realistic dispersal rate of 1.5 km/year for birds and mammals and 0.1 km/year for reptiles, amphibians and plants. The projected velocity of temperature change over the earth's surface is estimated to be 0.42km/yr (0.11-0.46 km/yr) for the 2050s, whilst observations over the period 1950-2009 already show median velocities of 2.7 km/yr (on land) and 2.2 km/yr (in the ocean) over the period 1950-2009. While these dispersal rates suggests that birds and mammals may be able to keep up with climate change, recent work has found

that even birds are lagging behind the climate change in some areas. Most plants, reptiles and amphibians would lag well behind the current climate change velocity.

3.2 Simulations performed

The climate data used to develop the models came from CRU TS 3.22 for developing the models (elevation interpolated using spline smoothing to 20km x 20km). An initial set of climate change model runs were performed using data from ClimGen (see WP 2) using global temperature time series. The global temperature time series that match the Representative Concentration Pathways (RCPs) used in this project were kindly provided by the UK Met Office Hadley Centre. They are identical time series to those used in the AVOID2 (Avoiding Dangerous Climate Change) project funded by the UK Department of Energy and Climate Change (Bernie & Lowe, 2014). These time series encapsulate the uncertainty in GCMs through the process described below. They are probabilistic outcomes of the modelling system used in AVOID2, which samples scientific uncertainties in the climate system by sampling distributions of physical parameters which have a dominant contribution to uncertainty in climate projections. The three physical parameters used in developing the scenarios are: the equilibrium climate sensitivity (ECS), which is the long-term warming response to a doubling of atmospheric CO₂; ocean diffusivity, which affects how quickly heat is removed from the upper ocean, moderating the rates of atmospheric warming; and climate-carbon cycle feedback strength, which accounts for how strongly climate change affects the ability of the carbon cycle to remove CO₂ from the atmosphere. The distribution of carbon cycle feedback uncertainty was based on Friedlingstein et al. (2006). The ECS distribution used is based on the IPCC Fourth Assessment Report (AR4, IPCC 2007a) and is a simple combination of ECS distributions from a number of alternative lines of evidence (Rogelj et al. 2012). The estimated distribution of ocean diffusivity is based on climate models from the IPCC AR4 (Gohar et al. 2011).

The Met Office calculated 10%, 50% and 90% probability outcomes for each of the four RCP scenarios as time series over the 21st century, expressing this as the global temperature rise relative to a 1961-1990 baseline. The scenarios run in the development of the biodiversity models used the patterns for 21 climate models and the 50th percentile PDF scenarios for RCP 2.6, 4.5, 6.0, and 8.5 and an additional 90th percentile run of RCP 8.5 for a 6°C world. A total of 110 runs have currently been completed and the results are outlined below.

The biodiversity modelling requires booking time on several High Performance Computing Clusters and making large amounts of disk storage available. While the high resolution model scenarios will be run with the biodiversity models, delays in receiving the complete set of data (difficulty in booking time on the systems required means that we can only do this once more) means that the high resolution Helix model runs have not been run with the biodiversity models yet. The next time slot that may be available for these runs is in the February – March time period and the model runs are slated to be run before the end of the project. Future papers from these analyses can also then compare results from high end temperatures from pattern scaling compared to high resolution climate models run through an impact model – an additional product spanning WP 3 and 4.

3.3 Results

One of the main goals of the Wallace Initiative is the identification of climate “refugia” – areas projected to become climatically unsuitable for the fewest species to climate change. Knowledge of these areas provide the best opportunities for “no regrets” natural resource management. These are the areas where climate change potentially has the least impact on species, so business-as-usual conservation may be most effective. The definition of a refugia adopted by the Wallace Initiative is an area that remains climatically suitable for more than 75% of the species modelled in that area. The other advantage of this approach is that it allows a better understanding of uncertainty as it allows for the production of maps showing the number of climate models in agreement that a given region would be a refugia. The flip side of this, and one becoming more important at higher temperatures, is termed an

“area of concern” (AOC). AOCs are areas projected to become climatically unsuitable for >75% of the species studied. Clearly, the potential loss of more than 75% of the species in an area is an indication of large-scale ecological transformation with concomitant impacts to ecosystem services. However, even the potential loss of 25% of the species in an area could have significant impacts. Finally, maps and graphs are provided showing the average percentage of current species potentially at risk (i.e., percent of species whose modelled climate becomes unsuitable) under 2° - 6°C of warming.

The sample maps presented below (Figures 3.1 to 3.3) are for plants with no dispersal. For this study more than 50,000 plant species were each individually modelled and the results presented here are aggregations of these data (as outlined above). Birds, mammals, reptiles and amphibians have also been modelled and summary results will appear on Helixscope in due course, as well as results being submitted to peer-reviewed journals. In this case the no dispersal scenario is being presented as it allows looking at 1.5° of warming (outside of the original design of Helix but of policy relevance now) and as it represents, to some extent, a ‘worst case’. However, as the dispersal rate of plants, on average, is low (see above), and there are barriers to movements in many areas (e.g., cities, road networks, agriculture), it is not an unreasonable approach.

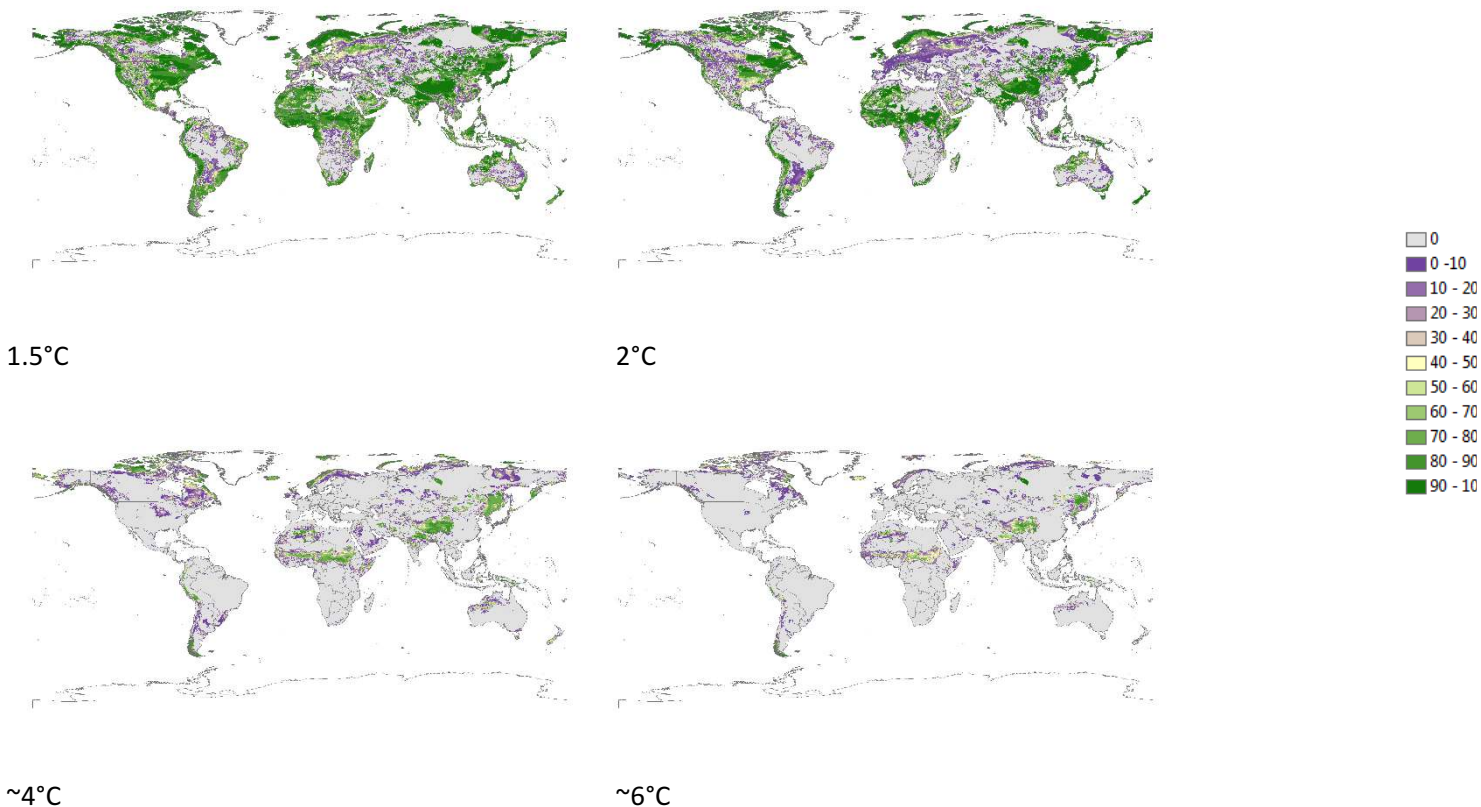


Figure 3.1 Potential impacts of differing levels of climate change on plant refugium. Scale is percentage of models projecting that a given 20km x 20km cell remains climatically suitable for more than 75% of the species modelled.

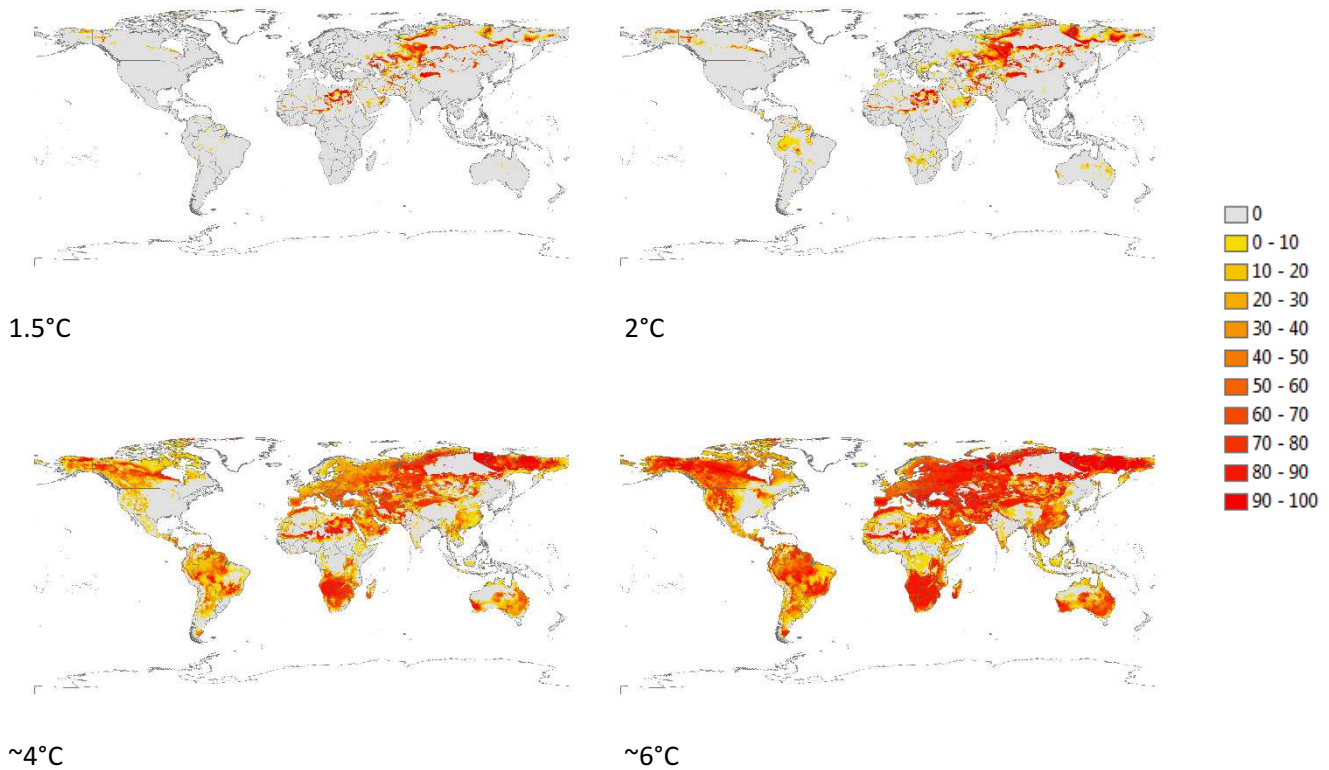


Figure 3.2 Potential impacts of differing levels of climate change on plant Areas of Concern. Scale is percentage of models projecting that a given 20km x 20km cell becomes climatically unsuitable for more than 75% of the species modelled. An Area of Concern can be viewed as an area at potential risk of undergoing a substantial change and/or degradation in the ecosystem and its functioning.

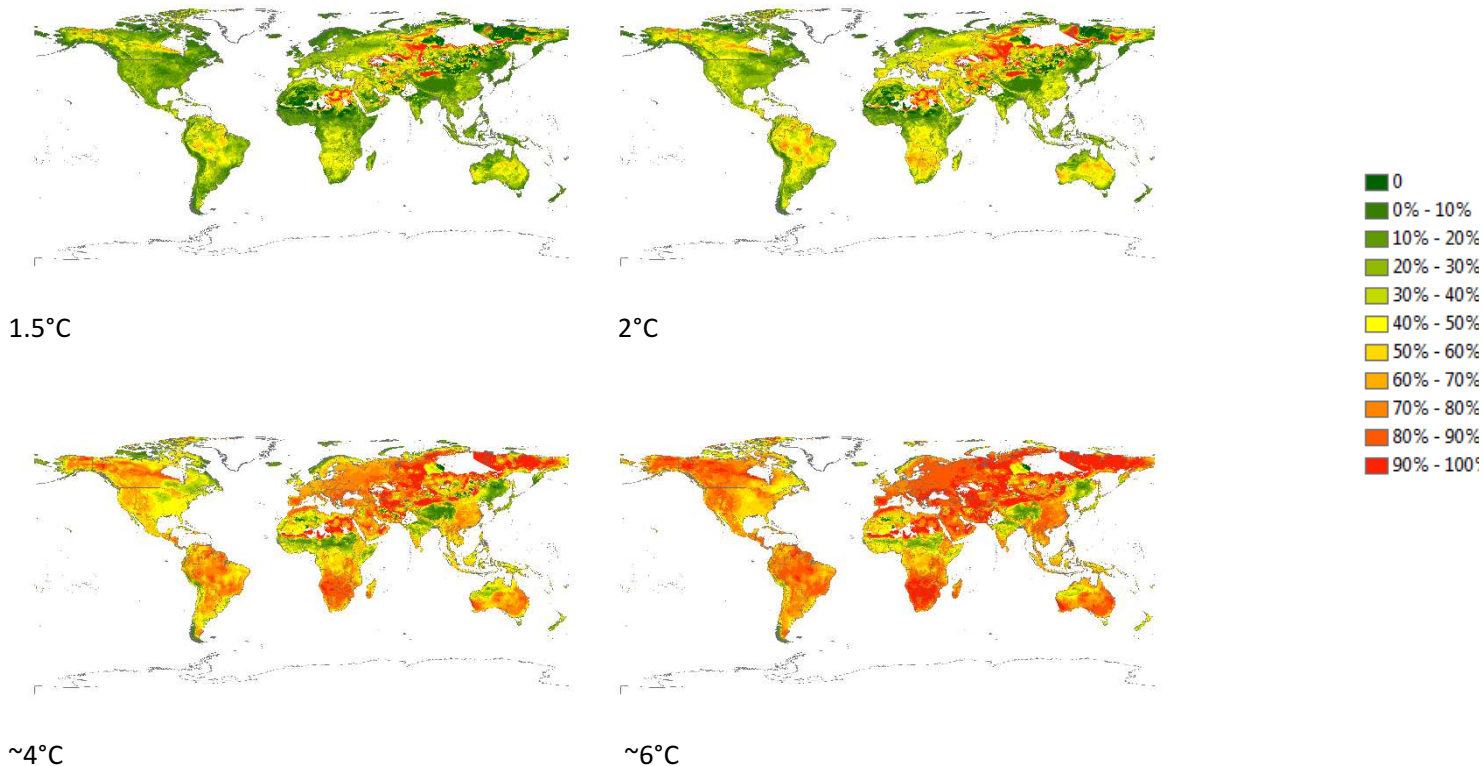


Figure 3.3 Potential impacts of differing levels of climate change on plant species richness. Scale is percentage of species currently present in a given 20km x 20km cell potentially at risk of extirpation owing to the local climate becoming unsuitable for those species at that level of warming.

3.4 Discussion

The three figures above show three different ways of looking at the potential impacts of climate change on biodiversity. Figure 3.1 looks specifically at those areas likely to remain climatic refugia for plant species under increasing levels of warming. This figure shows that even with 1.5° of warming there are some areas (in gray) with the local climate potentially becoming unsuitable for more than 25% of the species modelled, including parts of the Amazon and southern Africa. These areas are more extensive with 2° of warming, covering most of the Amazon and southern Africa. This does not mean that the area is 'lost' (see Figures 3.2 and 3.3), just that it is likely already undergoing some levels of change to different plant species. However, there is a tipping point between 2° and 4°C such that very few areas are plant refugia by 4°C of warming and this decreases more by 6°C (some remaining refugia likely in high mountain areas of the Andes and also the Southern Cone of Chile).

Figure 3.2 looks for the areas with the greatest potential impacts in terms of increasing levels of climate unsuitability for plant species. These are areas where the climate is projected to become unsuitable for more than 75% of the species modelled. As might be expected, with 1.5°C of warming there are few areas beginning to become unsuitable. Those that are tend to be more extreme climates with fewer species modelled. However, by 2°C of warming some areas in the Amazon, southern Africa and elsewhere are projected to become Areas of Concern, at least under a few climate models. However, as with refugia, the tipping point for many parts of the World appears to be between 2° and 4°C. With approximately 4°C of warming large areas in South America, Canada, Europe, Russia, southern Africa and southern Australia are becoming climatically unsuitable for large numbers of plant species. By the time warming reaches 6°C, very few areas are not projected to be undergoing significant amounts of ecosystem change (as measured by plant species). This is further by looking at Figure 3.3, which shows some level of impact on all

terrestrial land sources, most of which shows projected climatic unsuitability for greater than 40%-50% of the species modelled.

While the projected impacts on birds and mammals is not as great (not shown), especially with dispersal factored in, the projected level of changes in habitats is such that the overall impacts on biodiversity, ecosystems and ecosystem functioning under 6° of warming is high. These are largely not 'instantaneous' changes. Many plants are long-lived and there would be expected to be a lag between reaching a warming level and the final ecosystem state which will be determined by factors such as longevity, disturbance rates and magnitude, and dispersal rates of replacement species. However, recent observations in the western United States have shown that extreme drought rapidly increases the likelihood of tree mortality and loss through insect outbreaks and fires. These sorts of changes indicate that in many areas there may be a transition to shrubby, or weedy, stage between two forest types and that these may very well be occupied by invasive species and have lower biodiversity and ecosystem services than either the current, or eventual future ecosystem state.

The potential inability of species to track shifting climates poses new and serious risks to species and ecosystems. Species for which dispersal is limited by natural barriers (e.g. island endemics), anthropogenic barriers (e.g. transformed land), inherent biological characteristics (e.g. morphological, behavioural or physical traits), disappearance of suitable climate conditions, or their reliance on other organisms or habitats that shift at different rates, are at increasing risk of endangerment (Root & Schneider 2006; Williams and Jackson 2007; Williams et al. 2008). Range shift limitations can be further exacerbated by human responses to climate change, for example changing land-uses (Kostyack et al. 2011). In large regions, particularly in the tropics, climate change is predicted to generate conditions unlike any occurring today (J. W. Williams et al. 2007); the risks and ecological implications of species reshuffling into novel, no-analogue communities are, as yet, unknown (Root & Schneider 2006; Williams & Jackson 2007).

While bioclimatic models have sometimes been challenged as an approach to examining the large scale impacts of climate change on large number of species they remain an often used approach. Even mechanistic models, based on physiology, are limited because the knowledge on the physiology or requirements of a given species varies over its range and different populations. Even a species' habitat requirement (especially in birds) varies substantially depending on whether the population is in the core or edge of its range. All models have limitations. However, a recent meta-analysis (Urban 2015) found that bioclimatic models were often **more** conservative in their projections of change than traits-based models or models based on expert judgement.

However, almost all model estimates are likely to be conservative, owing to processes that are not included in the models which, overall, tend to underestimate the projected impacts. A key factor omitted from many models is the effect of extreme events (such as floods, seasonal droughts, or heatwaves, which can then in turn lead to fire for example), which are generally projected to increase in frequency and intensity as climate changes. This is important because species do not experience the mean climate – they experience a series of changing extreme events *around* the mean, and as those extremes become more extreme it is the experience of these that are likely to cause local extirpation. This is particularly important because climate change increases climate variability disproportionately compared to the mean (that is, if for example, the mean summer climate in a place becomes 2°C warmer locally, the heatwaves are likely to be more than 2°C warmer than previously experienced, and they are likely to happen more often). Whether species can recover or not from extreme events depends on how quickly the climate returns to 'normal' or how often the event in question occurs. In the few cases where extreme events, or adequate time series, have been included in a bioclimatic modelling study, the projected impacts were modelled to occur much earlier than models based on changes in the means. While certain traits may make some individual species more resilient to climate change (and research is just beginning to really tease out what these traits are), the lack of inclusion of extreme events suggests that many species may be more sensitive than once thought. This is because climate



change does not just change the mean climate in a given place, but also tends to increase the climate variability. Another key factor omitted is the tendency for changes, often increases, in the ranges of pests and diseases as the climate warms. These pests and diseases then impact on biodiversity and this is not included in the bioclimatic models. Even mechanistic models, based on physiology, that run at daily or yearly time steps often do not include disturbances such as pests and fire.

4. Biomes

Impact Model Used and Brief Description of experiments

ORCHIDEE is a process-driven Dynamic Global Vegetation Model (DGVM) designed to simulate C and water cycle from site-level to global scale (Krinner et al., 2005; Ciais et al., 2005; Piao et al., 2007). It is composed of two main modules. SECHIBA computes the energy and hydrology budget on a half-hourly basis, together with photosynthesis based on enzyme kinetics (Viovy et al., 1997). These results are fed to a module called STOMATE, which simulates C dynamics on a daily basis: gross primary production (GPP) is allocated to different organs, and then respired by the plant or by soil microorganisms when parts of the plant die. These processes determine several ecosystem state variables such as leaf area index (LAI) and canopy roughness, which are fed back to SECHIBA because they control the energy and water budgets. The equations of ORCHIDEE are described in Ducoudré et al. (1993) for SECHIBA and in Krinner et al. (2005) for STOMATE, and can be found at <http://orchidee.ipsl.jussieu.fr/>. As most DGVMs, the vegetation is described into a discrete number (13) of PFTs over the globe. For grassland, C3 and C4 grass are included, and treated like unmanaged natural systems, where C / water fluxes are only subject to atmospheric CO₂ and climate change. Recently, a more complex 11-layer soil-water diffusion scheme (De Rosnay et al., 2000, 2002; D'Orgeval, 2006, 2008) and the mechanistic intermediate-complexity snow scheme (ISBA-ES; Boone and Etchevers, 2001) have been implemented in ORCHIDEE Trunk.rev3623, which improves the representation of water and snow-related processes (e.g., Wang et al., 2013; Traore et al., 2014; Guimberteau et al., 2014). Dynamic vegetation scheme was activated in the HELIX WP4.4 simulations, which allows the vegetation dynamics driven by the climate change.

Simulations were performed for the following forcings for both transient and time slices for SWL of 1.5, 2 and 4K (see also Table 4.1): EC-EARTH3-HR + IPSL-CM5-LR (r1), EC-EARTH3-HR + GISS (r5) and HadGEM3-HR + IPSL-CM5-LR (r1)

Table 4.1 List of simulations performed with ORCHIDEE for quantification of impact on biomes

Climate model	GCM ensemble	Type	CO ₂ (ppm)	Period
EC-Earth3-HR	r1i1p1	Transient	RCP85	1971-2070
		SWL1.5	401.628	2016-2065
		SWL2	448.835	2031-2080
		SWL4	661.645	2068-2119
EC-Earth3-HR	r5i1p1	Transient	RCP85	1971-2130
		SWL1.5	421.864	2023-2072
		SWL2	480.508	2039-2088
		SWL4	954.466	2013-2062
HadGEM3-HR	r1i1p1	Transient	RCP85	1971-2070
		SWL1.5	401.628	2016-2065
		SWL2	448.835	2031-2080
		SWL4	661.645	2068-2119

Results

Compared to the baseline period (1986-2005), ORCHIDEE DGVM projected large increase in global GPP under future climate change. GPP increases along further warming (Figure 4.1). For SWL of 4K, the global annual GPP was simulated to increase by 44% to 75% compared to baseline period. The largest increase was modeled driven by GISS-E2-H, mainly due to the much higher CO₂ concentration when SWL of 4K was reached by GISS-E2-H GCM (at 2102; 954 ppm CO₂ concentration) than by IPSL-CM5-LR GCM (at 2068; 662 ppm CO₂ concentration). In addition, when

driven by different climate forcings, significant difference in the modelled GPP and its future changes were found (Table 4.2), indicating both GCM and high-resolution model could impact the productivity projection.

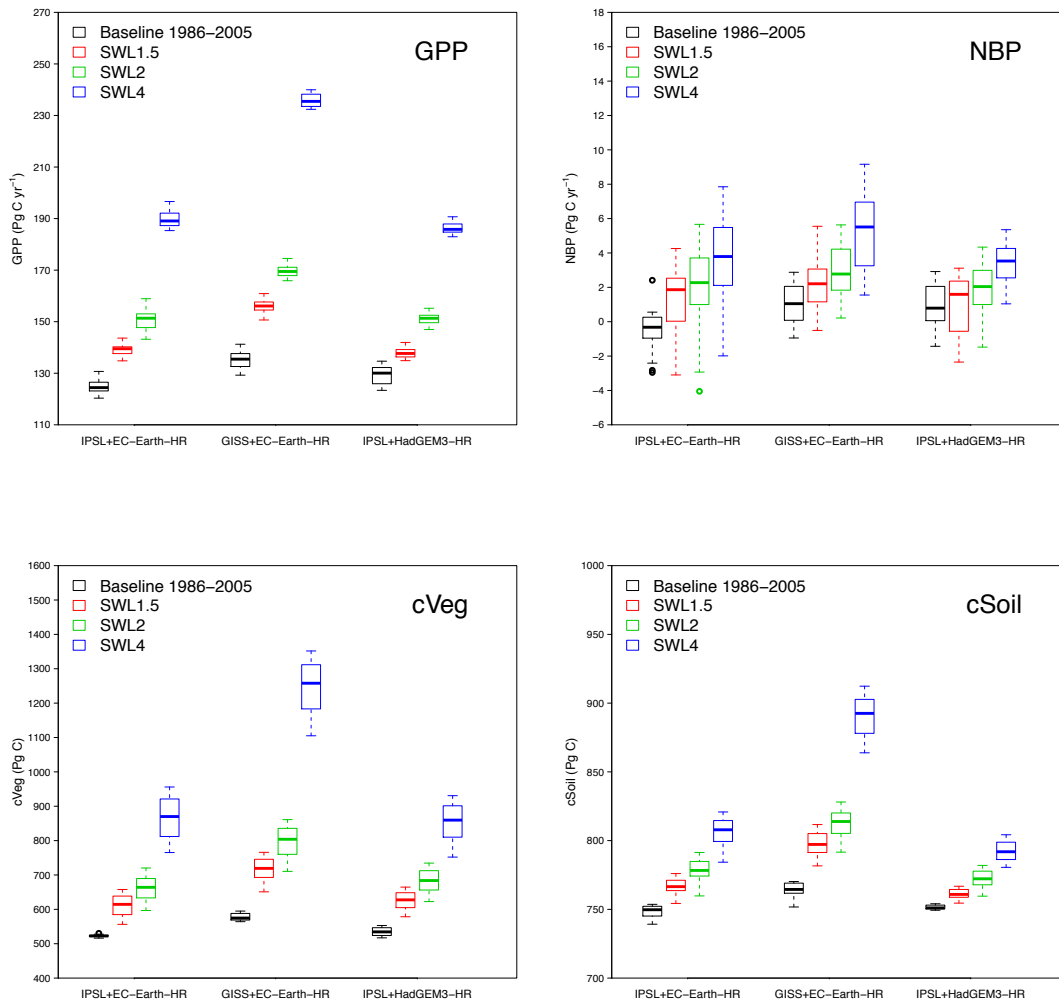


Figure 4.1. Global GPP, NBP, cVeg and cSoil for baseline (1986-2005) and for SWL of 1.5, 2 and 4K simulated by ORCHIDEE model driven by different high-resolution climate forcings.

Table 4.2. Global GPP, NBP, cVeg and cSoil for baseline (1986-2005) and their changes for SWL of 1.5, 2 and 4K relative to baseline.

	Run ID	SSTs	HR model*	Baseline#	Changes relative to Baseline (%)		
					SWL1.5	SWL2	SWL4
GPP (Pg C yr ⁻¹)	R1	IPSL-CM5-LR	EC-Earth-HR	125 ± 3	11	21	52
	R2	GISS-E2-H	EC-Earth-HR	135 ± 3	16	26	75
	R3	IPSL-CM5-LR	HadGEM3-HR	129 ± 4	7	17	44
NBP§ (Pg C yr ⁻¹)	R1	IPSL-CM5-LR	EC-Earth-HR	-0.5 ± 1.3	1.4 ± 1.7	1.9 ± 2.3	3.7 ± 2.2
	R2	GISS-E2-H	EC-Earth-HR	1.1 ± 1.2	2.1 ± 1.3	2.9 ± 1.4	5.3 ± 2.0
	R3	IPSL-CM5-LR	HadGEM3-HR	0.9 ± 1.3	1.0 ± 1.6	1.9 ± 1.5	3.4 ± 1.0
cVeg (Pg C)	R1	IPSL-CM5-LR	EC-Earth-HR	523	17	26	65
	R2	GISS-E2-H	EC-Earth-HR	578	24	38	116
	R3	IPSL-CM5-LR	HadGEM3-HR	535	17	28	59

cSoil	R1	IPSL-CM5-LR	EC-Earth-HR	749	2	4	8
(Pg C)	R2	GISS-E2-H	EC-Earth-HR	764	4	6	16
	R3	IPSL-CM5-LR	HadGEM3-HR	751	1	3	5

*HR model is the high resolution climate model driven by the SSTs boundary conditions

#Baseline is 1986-2005.

§NBP value for different SWLs were shown rather than relative changes.

Driven by the modelled increasing GPP in the future, positive and increasing NBP (carbon sink) were simulated by ORCHIDEE DGVM under global warming (i.e., the accumulation of soil organic carbon, cSoil; Figure 4.1; Table 4.2). In addition, strong increases of total vegetation biomass (cVeg) were simulated for future global warming, which can be due to 1) the higher productivity, 2) forest regrowth in abandoned land, and 3) the forest expansion over current grassland or bare soil where forest could potentially be allowed under future global warming (e.g., Figure 4.4).

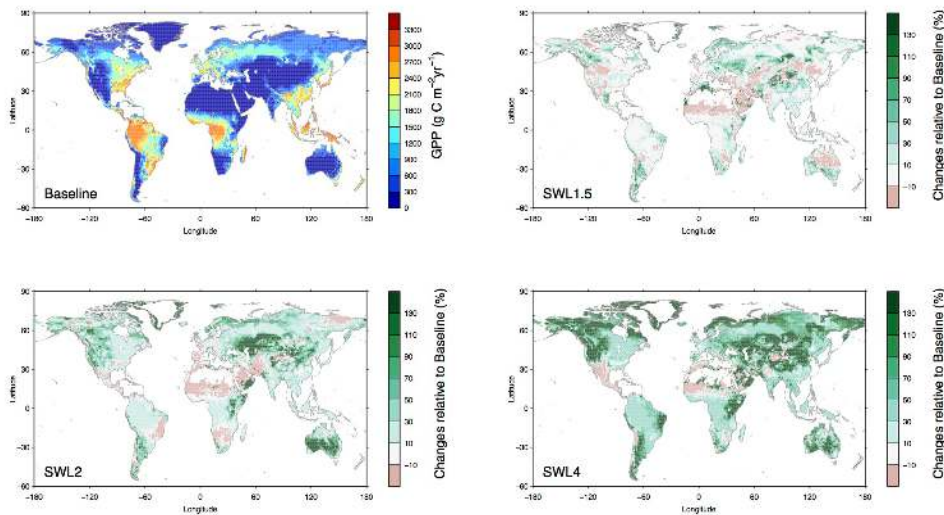


Figure 4.2. The spatial pattern of GPP for baseline (1986-2005) and its relative changes for SWL of 1.5, 2 and 4K simulated by ORCHIDEE driven by EC-Earth-HR-R1 (IPSL-CM5-LR SSTs) climate forcing.

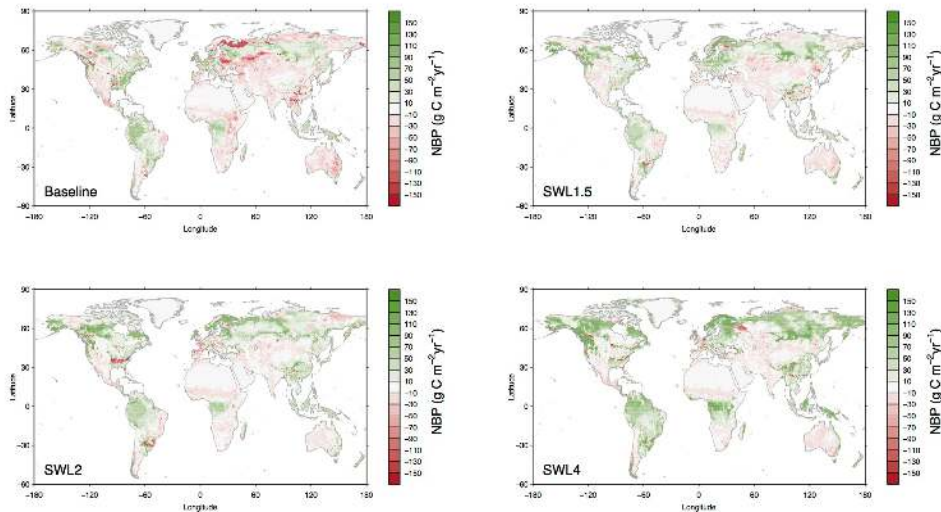


Figure 4.3. The spatial pattern of NBP for baseline (1986-2005) and for SWL of 1.5, 2 and 4K simulated by ORCHIDEE driven by EC-Earth-HR-R1 (IPSL-CM5-LR SSTs) climate forcing.

The increase in GPP for future global warming was projected over most of the terrestrial ecosystems (Figure 4.2). Strongest GPP increase was projected over mid-latitude semi-arid grasslands (e.g., western North America, central Asia, and southeast Australia) and North-Hemisphere high-latitude tundra. However, there are regional differences in the modeled GPP change depending on different climate forcings (data not shown). Driven by GPP increase, positive NBP was modeled over high-latitude regions under future global warming (Figure 4.3). The positive in NBP, however, did not always follow the increase GPP. For SWL of 1.5, 2 and 4K, strong positive NBP (carbon sink) was simulated over tropical forest regions and southeast China, where only moderate GPP increase was modeled. In addition, negative NBP (carbon source) was simulated over central Asia and inland southeast Australia, even though strong GPP increase was simulated at the same period, which indicates other processes rather than GPP play a major role in determine NBP over these regions (e.g., elevated heterotrophic respiration driven by climate, or fires cause by more frequent extremes).

The increase in the total vegetation biomass was simulated by ORCHIDEE DGVM (Figure 4.4), which can be due to 1) the higher living biomass because of the higher productivity, and 2) the forest expansion over current grassland or bare soil where forest could potentially be allowed under future global warming (e.g., arctic regions in Figure 4.5).

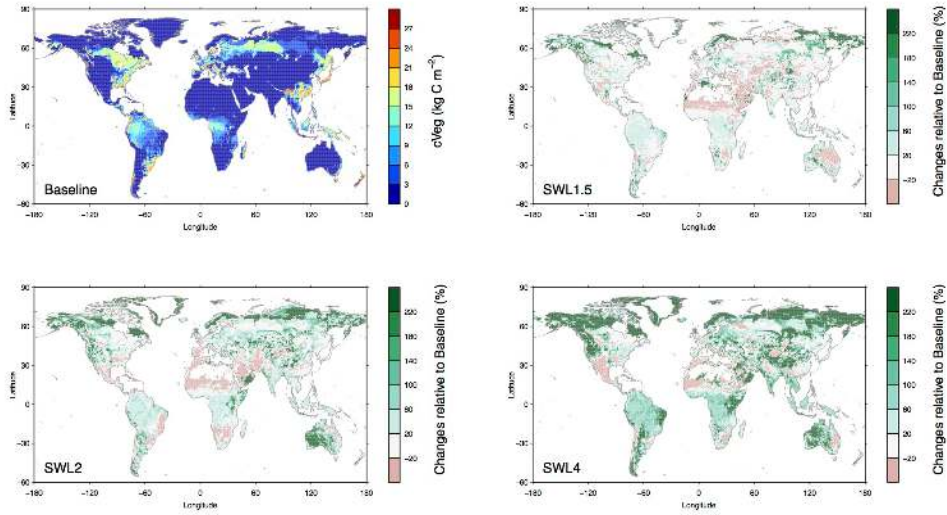


Figure 4.4. The spatial pattern of total vegetation biomass (cVeg) for baseline (1986-2005) and its relative changes for SWL of 1.5, 2 and 4K simulated by ORCHIDEE DGVM driven by EC-Earth-HR-R1 (IPSL-CM5-LR SSTs) climate forcing.

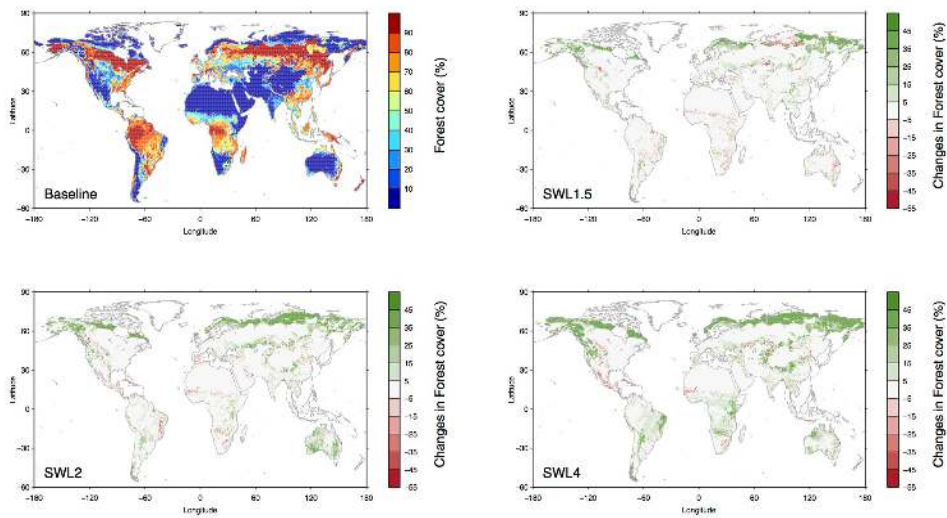


Figure 4.5. The spatial pattern of forest coverage for baseline (1986-2005) and its changes for SWL of 1.5, 2 and 4K simulated by ORCHIDEE DGVM driven by EC-Earth-HR-R1 (IPSL-CM5-LR SSTs) climate forcing.

5. Drought

6.1 Introduction

Droughts result from a shortfall in precipitation over an extended period of time or from the inadequate timing or the ineffectiveness of the precipitation, often combined with high temperatures and increased water demands. It is a complex disaster due to its often long persistence and the propagation through the entire hydrological cycle.

While droughts are known to affect extended areas and a large number of people, the related impacts are often difficult to quantify: they are non-structural and spread over larger areas and longer periods than damages resulting from other natural hazards such as floods or forest fires (Wilhite 1993). These characteristics make it difficult to evaluate and quantify the damage caused by single drought events. While negative socio-economic impacts are frequently reported for agricultural production, public water supply, tourism, power generation, and other water-dependent industries, environmental impacts related to water quality, wetlands and biodiversity that in the long-run may lead to environmental degradation, are more difficult to quantify (Vogt and Somma 2000, Maia et al 2014).

Disaster impacts can be measured in terms of losses or damages, where the term loss represents negative economic impacts (measured in monetary units) while the term damage refers to the total or partial destruction of physical assets in the affected area (Smith and Ward 1998, de Groeve et al 2014). Damages occur during and immediately after the disaster and are measured in physical units. Their monetary value, the related loss, is expressed in terms of replacement costs according to prices prevailing just before the event (ECLAC 2003). Based on these concepts the risk resulting from a certain natural hazard can be evaluated. Brooks (2003) provides a comprehensive review of the various risk definitions to be found in literature. Most of them are based on approaches combining the probability of hazard occurrence and the likely impacts of a resulting disaster, which depend on the severity of the event and on the exposure and vulnerability of the socio-economic or natural system affected. In order to assess the potential impact of an ongoing or possible future drought event, quantitative information on both the severity of past events and on their related impacts (damages or losses) are, therefore, required.

Extreme Value analysis are carried to compute the severity and recurrence of droughts covering the historic baseline, 1.5°C, 2°C, and 4°C warming level conditions for different return periods. Assessment of the drought risk that covers hazard and exposure in terms of the expected annual exposed population and assets. Drought severity results are combined with scenario estimates of GDP and population density (shared socioeconomic pathways or SSPs, van Vuuren and Carter, 2014) to estimate the expected annual exposed.

The strategy of considering changes in drought properties for the specific warming levels (+1.5°C, +2°C and +4°C with respect to pre-industrial conditions) is mainly oriented to better assist decision makers to set targets to prepare mitigation plans for the different plausible targets of warming. Moreover, for impacts that are linked with the increase of global temperatures, this approach could reduce the net uncertainty due to scenario and climate sensitivity. As a drawback, this approach might highlight the uncertainties related to the response of the climate system to the human-induced changes (Swain and Hayhoe, 2015). Usually the date of reaching the different warming levels is earlier for the more sensitive models (IPSL-CM5A-LR/MR, EC-EARTH, HadCM3LC) and latter for the less sensitive (GFDL-ESM2M, HADGEM2-ES, GISS-E2-H).

The changes in the probability of occurrence of extreme droughts was assessed globally using the Standardized Precipitation Index (SPI) and Standardized Precipitation-Evaporation Index (SPEI). Both indicators were computed using precipitation and potential evapotranspiration (LISVAP) simulations over the period 1970-2100. Derived variables like changes in frequency, duration and severity of droughts were used for drought characterization. The changes between present climate and projections were assessed by computing the differences between drought

characteristics derived from the baseline defined as the 1970-2005 period. Generally, the wet and dry areas are quite similar among the different models for the different warming levels.

6.2 Data and methods

The aim of this research is to evaluate the implications of climate change on future drought risk at global scale. For different warming levels changes in the expected annual drought damage and people affected were estimated. The goal proposed to extrapolate current drought losses to future time periods, taking into account changes in climate (high levels of warming) and socio-economic dynamics.

The analysis is based on a set of seven climate projections with high concentration scenario (i.e., RCP 8.5) produced with EC-EARTH3-HR v3.1 by the Swedish Meteorological and Hydrological Institute (SMHI). Projections are obtained by forcing EC-EARTH3-HR with Sea Surface Temperature (SST) and sea-ice forcing from independent driving GCMs. The benefits of downscaling the models output with EC-EARTH3-HR are to render uniform and increase the spatial resolution, from the original grid to 0.35°, leading to an improved characterization of extreme events and to comparable statistics among different models.

Droughts of a certain magnitude or recurrence frequency may impact over one or several sectors, however the magnitude of the impact varies depending on the spatial distribution of exposed assets or population and with the magnitude of the event. For example, in certain regions a 10-year drought may have serious impact, in other regions such events may have no impact. Ideally one would construct (at country or region level) a set of damage curves linking the magnitude of any specific event (in terms of SPI or volume of water in river) with a certain damage based on observed events and reported damages. From disaster loss records and an extreme value analysis of climatology for each corresponding time window could be possible to construct such damage curves relating occurrence probability with damage. The expected annual damage then equals the integral of the damage-probability curve. For future time windows related the specific levels of warming one would then evaluate the changes in probability of occurrence of the present 2, 5, 10, 20, 50 and 100 year events and obtain a new damage-probability curve (the link "magnitude event - impact event" remains the same, but the probability of occurrence of a drought with a certain magnitude changes under future climate). However for many regions in the world there is insufficient drought impact data to construct such curves and some more theoretical assumptions are needed.

The overall impacts of droughts on the assets, population, or natural ecosystems of a particular region depend on complex interactions and their cascade effects. A useful conceptual framework for risk (R) assessment is based on the combination of an external factor, defined by the severity of a natural phenomenon threatening the social system (hazard) on the one hand, and on the internal capacity of a society or ecosystem to cope with, resist to, and recover from a certain impact (vulnerability) on the other hand (UNDP 2004, IPCC 2007b, IPCC 2012, Naumann et al 2015). If the hazard is defined as the expected average number of events of a certain severity (N), and D is the expected average damage caused by an event of a certain severity (Hergarten 2004, Merz et al 2009) then the drought risk can be considered as the product of hazard and expected damage:

$$RISK = ND$$

This relation determine the risk of a drought of a certain severity in a given region and period of time, assuming a stationary relationship between hazard and expected damage. The assumption of stationarity can limit the accuracy for future projections since changes in the relationship between indicator and damage, for example through adaptation or improved mitigation measures, will result in larger uncertainties when projecting future damages.

Considering all the possible events, N can be represented by its cumulative probability density function P(s) where s represents the drought severity. The magnitude of s in this context can, for example, be defined as the absolute or

relative drought severity, the area affected by a drought of a certain severity, or by a bivariate probability function of both variables.

Following the formulation in Hergarten 2004 and Naumann et al., 2015 let $p(s)$ be the probability density of an event of severity “ s ”

$$p(s) = \frac{-P(s)}{ds}$$

and $D(s)$ the expected damage. The expected overall annual damage is then given by

$$EAD = \int_p D(p)dp$$

Finally the total drought risk can be determined by

$$R = N \cdot EAD = N \int_p D(p)dp$$

It follows that risk assessment relies on two main processes: the identification of a suitable distribution that can represent the drought events (hazard) and the assessment of the overall damage as a function of the drought severity where possible.

In this context, drought severity is defined as the sum of the absolute values below zero of the selected drought indicator during a given drought event. From the resulting time series, drought events have been identified from the month when the indicator falls below a given threshold until it reaches a value of zero again. Indicators were averaged at country or regional level in order to coincide with the spatial resolution of the impact data that were available only at country level. This aggregation can introduce an uncertainty in the data on drought severity, especially for large countries when only parts of the territory are affected. While spatially more resolved impact data would be desirable, such data are currently not available at global scale.

Analytical computation of EAD

The expected annual damage (EAD) of a given year is the integration of the drought risk density curve over all probabilities. Denoted by $D(p)$ the damage which occurs at the event with probability p . As depicted in the previous section, the EAD can be expressed as

$$EAD = \int_p D(p)dp$$

This integral is solved for the return period of $T(D(p))=0$, when no damage occurs at this event and with a probability of $p(D(p)=0)$ to the infinitely large event associated to a probability of zero.

Generally and mainly due to data constraints it is not possible to simulate the damage cost for all events between $T[D(p) = 0]$ and $T = \infty$. Therefore some approximation must be done in order to calculate the EAD.

Some analysis are found in the literature linked with this issue. The framework presented by Zou et al 2012 recommends the use of a log-linear relation between the return period and the damage costs which enable only very few simulations of the hazards and corresponding costs to be carried out. Using a log-linear model to represent

exceedance series is frequently used in hydrology for floods assessment (Apel et al 2004). Blauhut et al. (2015) applied annual impact occurrence based on reported information of droughts to estimate the drought risk as the probability of impact occurrence as a function of the Standardized Precipitation Evapotranspiration Index (SPEI). Blauhut et al. 2016 proposes a hybrid approach merging drought indices (mainly SPEI) and vulnerability factors to predict annual drought impact occurrence using a multivariate logistic regression. Naumann et al. 2015 proposed the use of power-law damage functions to assess the relationship between drought severity and related damages in two specific economic sectors across Europe. The resulting damage functions parameters are related by the specific drought vulnerability or adaptive capacity of each sector and country.

A plausible way for calculating the EAD, is a numerical integration of all probable return periods. The EAD can be calculated by integrating drought damage over all probabilities. This is done by combining the cost of n return periods where both hazards and costs have been estimated. Several different methods for numerical integration could be used. Here we used the trapezoidal rule:

$$EAD = \frac{1}{2} \sum_{i=1}^n \left(\frac{1}{T_i} - \frac{1}{T_{i+1}} \right) (D_i + D_{i+1})$$

Where n is chosen to cover all relevant return periods from negligible costs of quite frequent event and to very rare events.

The risk assessment focuses on direct tangible damages related to the impacts to physical assets, the disruption of productivity and loss of primary sources due to droughts observed and reported. Expected Annual Damages are obtained from the combination of climate hazard, and recorded drought costs and are expressed in 2010 US\$ assuming no socio-economic change in future scenarios, it means that modelled economic effects of future climate change are based on the current economy (quasi static analysis)

Climate model variability was quantified by the coefficient of variance of the future return periods retrieved for the different climate realizations. The significance of the changes in climate hazard was evaluated by the Kolmogorov-Smirnov test applied on the annual values of future time windows versus baseline, separately for each climate model.

In the case of a drought event, the meaning of exceedance or exceeding is that the drought severity is exceeded after a certain threshold. Baseline annual damages (EAD_{base}) are obtained for each macro-region and then disaggregated at pixel level by the integration of multiple disaster datasets (EMDAT, Desinventar) and economic and population statistics (IIASA).

Disaster loss records for drought that occurred in the 1970-2005 period have been collected from EM-DAT and Desinventar databases. Information for each disaster include: hazard type, country, year and loss estimate (direct damages to asset and production interruption expressed in US\$ in the value of the year of occurrence). In a second step, all costs have been converted into 2010 US\$ by applying the consumer price index provided by the US bureau of labour statistics. As such, baseline damage values were obtained for each region. It is important to note that the baseline damages derived per country for each hazard reflect the total damage (as reported in the EMDAT and Desinventar databases) in that country. This total damage relates to impacts in all sectors.

The specific warming levels (SWLs) are defined as the first time the 30 year running mean of the global averaged annual mean temperature is above the specific warming level (SWL) i.e. the year indicated the center of a 30 year average (Table 1.1). The global averaged annual mean temperature is calculated as the annual mean near surface temperature over the global and relative to pre-industrial levels.

Briefly, the estimation of damages have been obtained by assessing the changes in the frequency and intensity of drought events for each specific warming level compared to the present based on an ensemble of climate projections; linking observed damages with the occurrence of drought events in the baseline period (1980-2010) and finally extrapolating observed drought damages to different levels of warming based on the change in the frequency distribution of drought events.

6.3 Results and discussion

A set of twenty macro-regions as defined by UN is used to depict the main results of our analysis at global scale (Figure 5.1). Even if these regions are wide and comprises several countries together, they reflect some socio economic similarities and are used as the first approximation for international organization in order to prepare or develop aid plans. Several systems already exists that coordinates effectively drought monitoring and early warning systems that includes famine early warning systems in the most vulnerable regions. These systems are effective tools that helps the multinational coordination of relief actions and mitigation plans usually based on such information as monitoring conditions, medium range forecasts and the evaluation of climate change implications.

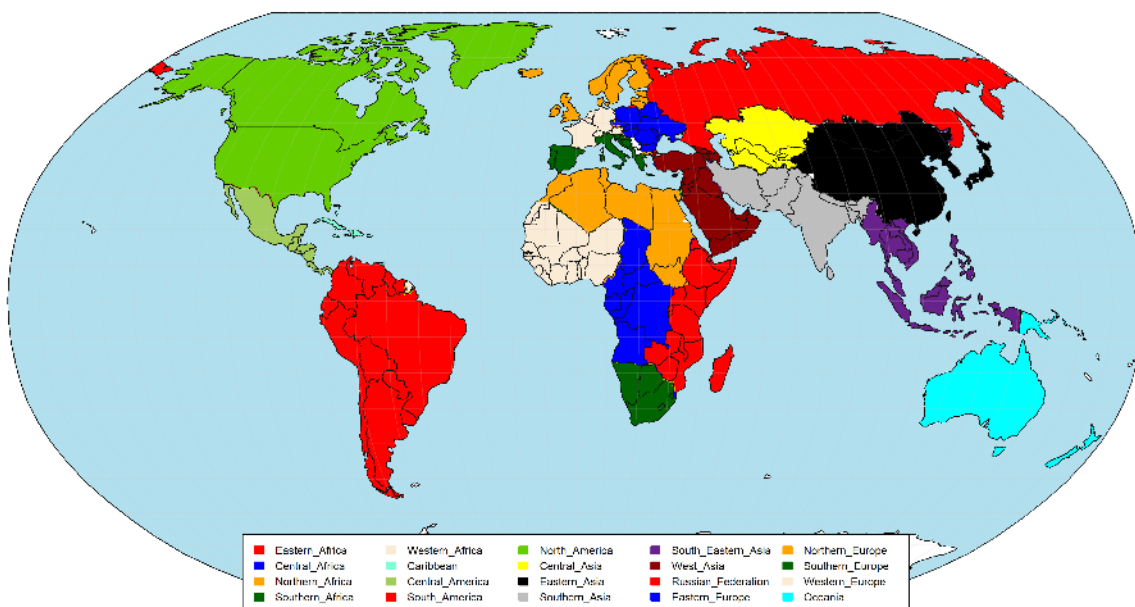


Figure 5.1 Composition of macro-regions as defined by UN.

Changes in the area covered by droughts is a straight measure of possible changes on risk as expected increases on the areas affected will directly increase the exposition of people and assets independently their preparedness or internal vulnerability. Figure 5.2 shows the drought severity evolution for the twenty different global macro-regions as defined by UN as represented in Figure 5.1.

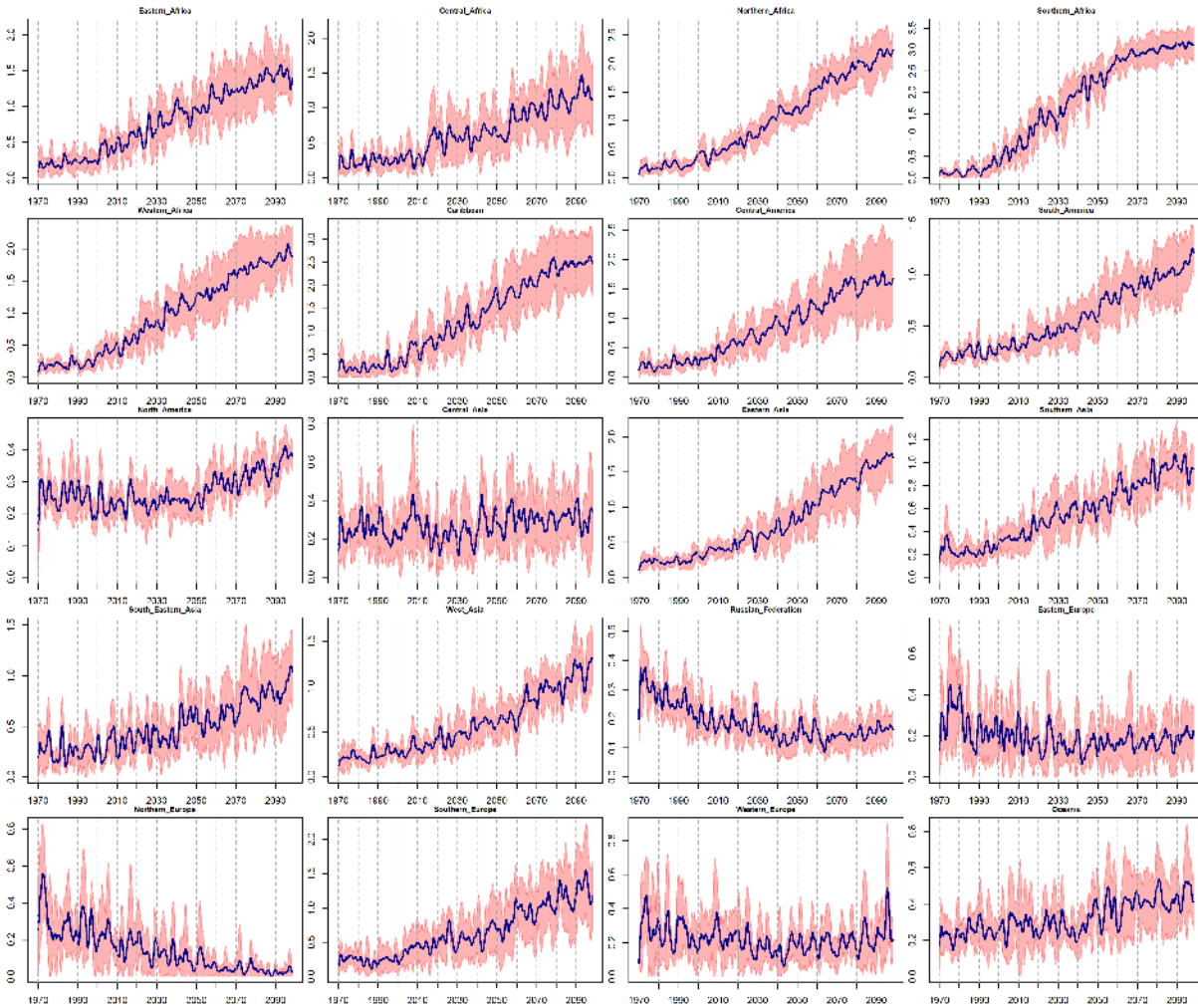


Figure 5.2 Drought severity for the different macro regions as defined in Figure 5.1. High level scenarios were used (RCP8.5). Based on SPEI – 12.

The typology of drought hazard representation is dependent on the drought indicator selected. No single drought definition exists and it is not possible capture all features of drought with a single indicator. Moreover, the use of diverse input variables (e.g., precipitation, potential evapotranspiration) might lead to some divergences.

However the indicators selected are among the most used globally, accepted by WMO for drought monitoring and are well linked with the most relevant impacts in terms of average annual losses and deaths (Naumann et al. 2015, Blauhut et al 2016). The metrics used to represent the selected hazards are crucial for the resulting impact scenarios: changes in return periods depend on the time scale selected or aggregation periods to characterize any event. Details on the sensitivity analysis and validation exercises for the drought indicators used can be found in (Naumann et al 2014, Bachmair et al., 2015).

This, linked with extreme value fitting may introduce additional levels of uncertainties in the projections of drought variables especially at high return periods. On that direction recent studies acknowledged its minor effect regarding the inter-model spread (Forzieri et al 2016).

Figure 5.2 summarises the main changes on severity for each macro region and the multi-model uncertainties. There it can be seen that consistent increase in the severity can be observed over most of the regions while the model spread tend to be larger in tropical areas like Central Africa or Central America.

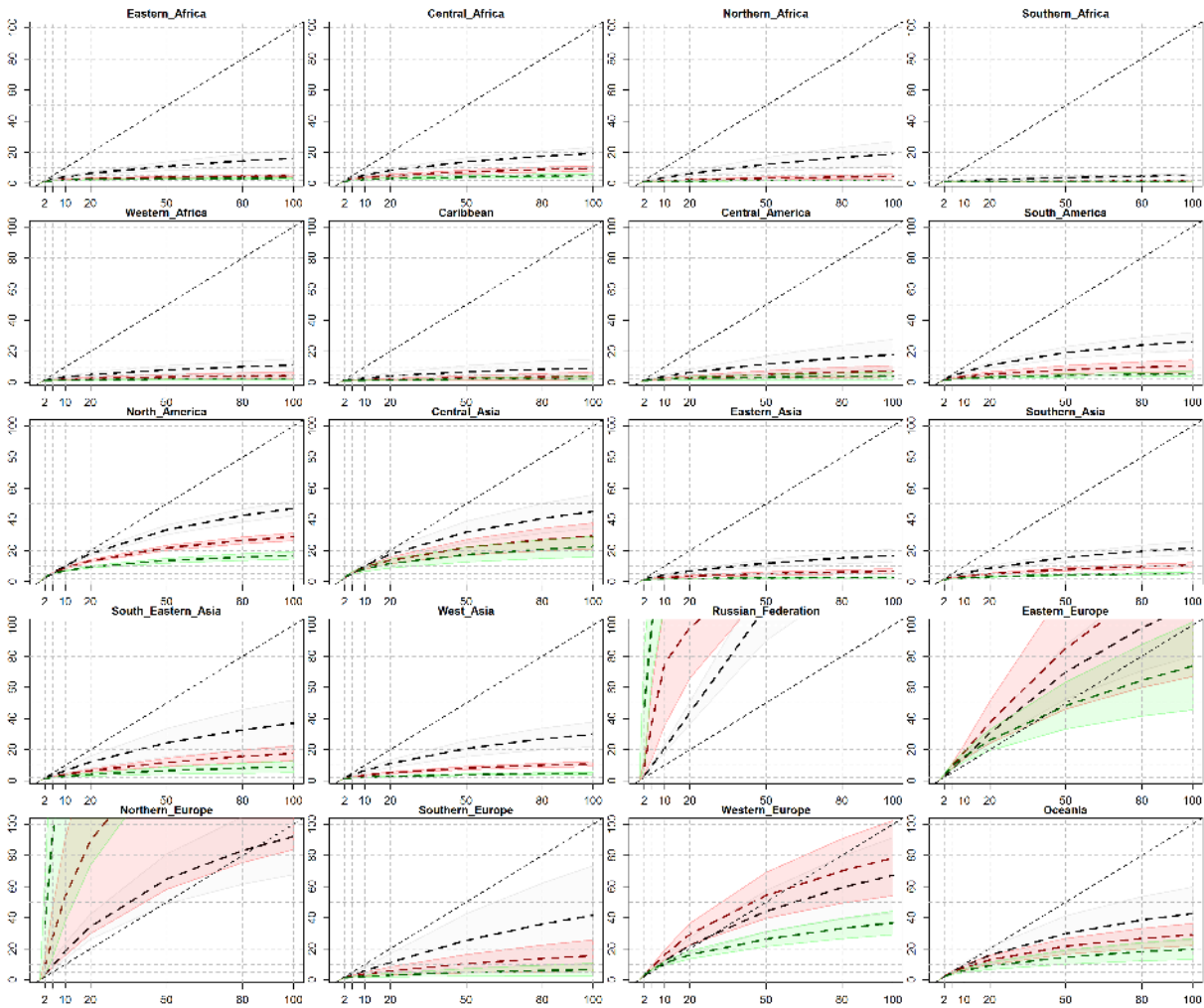


Figure 5.3 Changes in return periods of droughts in the different macro regions for 1.5°C (black), 2°C (red) and 4°C (green). Dashed black line represents the no-change curve. Data were computed at the pixel level and averaged over each region, also accounting for inter-model standard deviation (shaded areas).

Figure 5.3 shows the projected changes in frequency of droughts events with respect to current climate (horizontal axis). Increasing (decreasing) hazard occurrences are denoted by lines under (over) the identity line, the coefficient of variance (shaded areas) describes the inter-model spread uncertainty. Droughts may become more severe and persistent as a result of the reduction in precipitation and increased evaporative demands with higher temperatures as represented by PET. For instance, for some areas like Southern Europe, Southern and Eastern Africa current 100-yr. events could occur approximately every 2 to 5 years for warming levels of 4°C.

Economic annual damage is based on historical economic losses recorded from previous disasters. The EAD is disaggregated at pixel level by GDP shares within a country. The weights are an aggregate index relative to GDP within each macro-region.

Mainly our results show that drought damages for the present and for different levels of global warming compared with the pre-industrial levels reflect the impact compared with the present economy. Results show that drought damages will increase in most regions of the world with global warming, and that the magnitude of impacts are strongly related to the level of warming.

According to the present analysis (Figure 5.4), several regions in the world could face a significant increase in drought damages if warming levels will reach 1.5°C or greater warming levels. For instance, current damages of 50 million

US\$/year in South America are projected to multiply seven fold and rise up to 350 million US\$/year for the 4.0°C warming level (undiscounted and no socio-economic changes assumed). Similar rates of changes are projected for the other regions, however the level of uncertainty in the estimation is larger in regions where the effect of precipitation increase mask or compensate the effect of PET and make the estimation of return levels less robust. This is the case of Central Africa, Central Asia or Eastern Europe where the estimations of EAD for 4°C of warming could vary widely but doesn't overlap with the other warming levels.

Considering a static socio-economic scenario drought damages increase significantly in most of the macro regions analyzed. In Southern Europa, for instance, it could range from 61 million US\$/year in the present to 1 billion US\$/year by reaching 4°C (it represents the 1960 % respect to the baseline EAD). In Europe, droughts are one of the main responsible of the total economic damage due to weather and climate events with the largest share of future damages (more than 50%) due by droughts (Forzieri et al., 2016).

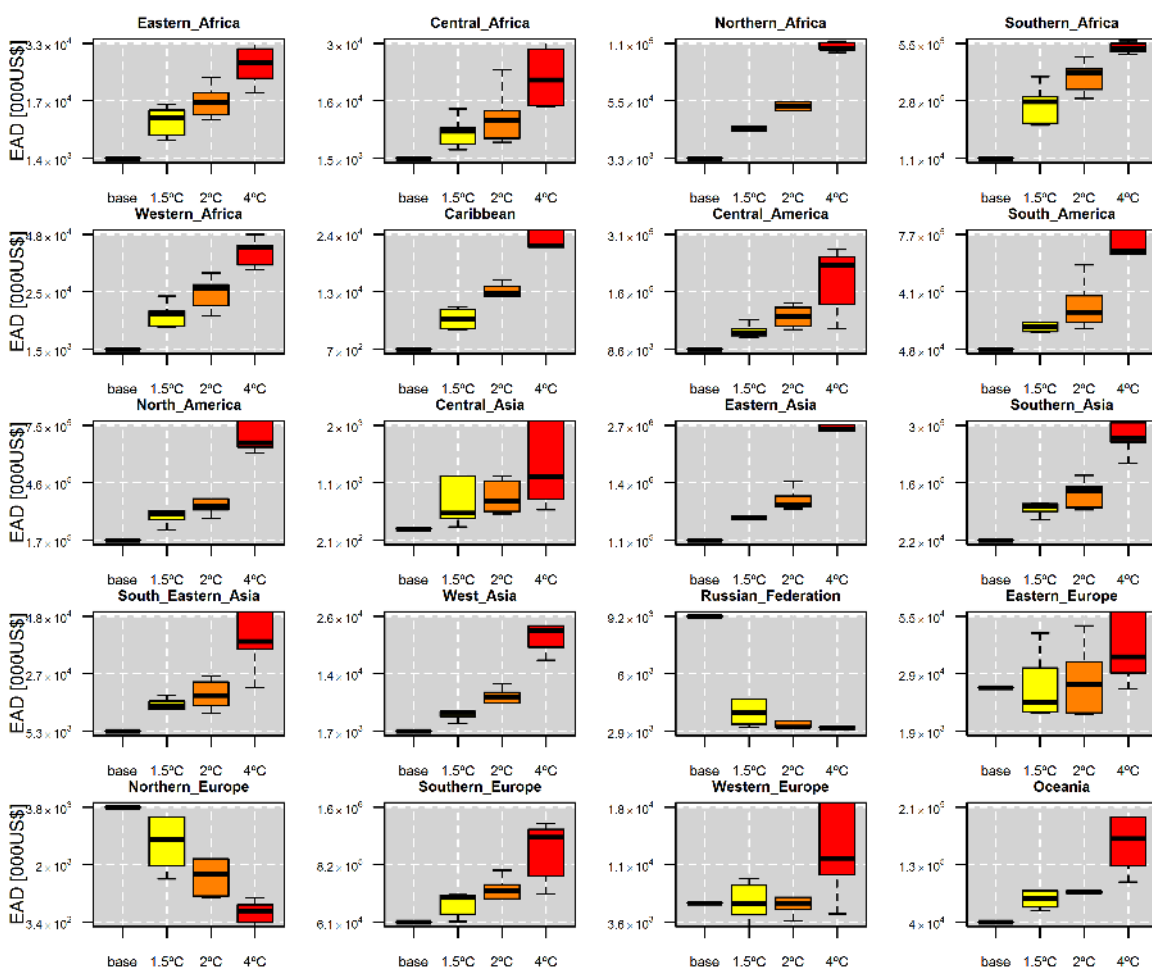


Figure 5.4 EAD [in thousand US\$] for the specific warning levels and different macro-regions and as defined in Figure 5.1. All estimates are using current GDP levels.

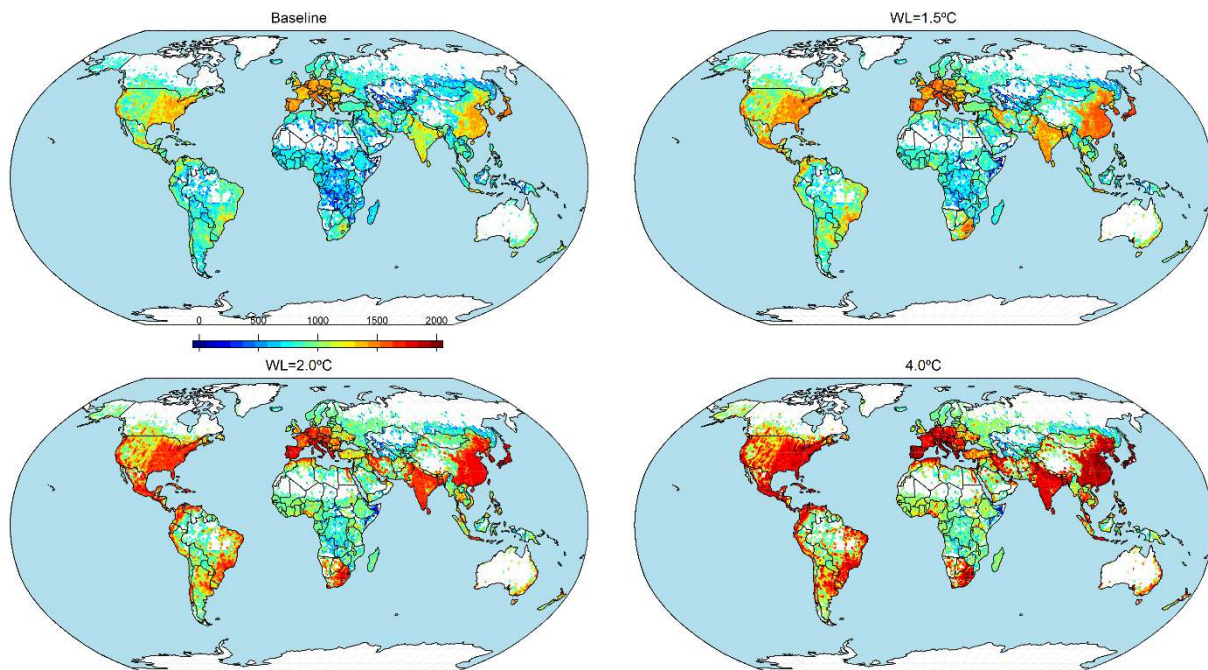


Figure 5.5. Expected annual losses due to drought [in thousand US\$] for the present (baseline) and the specific warming levels (1.5°C, 2.0°C, 4.0°C) according to seven different climate models and RCP8.5 scenario. Country losses are disaggregated according to gridded GDP values. All estimates are using current GDP levels.

Costs of droughts were disaggregated by GDP and population density to create a spatial distribution of costs (Figure 5.5). As noted above, the areas with the highest drought hazard areas often heavily exposed with dense populated areas and or high dependence of GDP on agriculture and other drought related sectors (Carrao et al., 2016). This make the greater economic losses be located in Europe, Eastern U.S., India and South East Asia, South Africa and South eastern South America.

Over those areas, the expected annual losses due to large events tend to increase up to 8-10 fold in the U.S., South Eastern South America, Southern and Central Europe and India and east China. This specific scenarios could be linked with an aggravated risk for global food security and potential for civil conflict in the medium to long-term. Since most agricultural regions show high infrastructural vulnerability to drought, then regional adaptation to climate change may begin through implementing drought protection infrastructure like fostering the widespread use of irrigation and rainwater harvesting systems (Carrão et al., 2016).

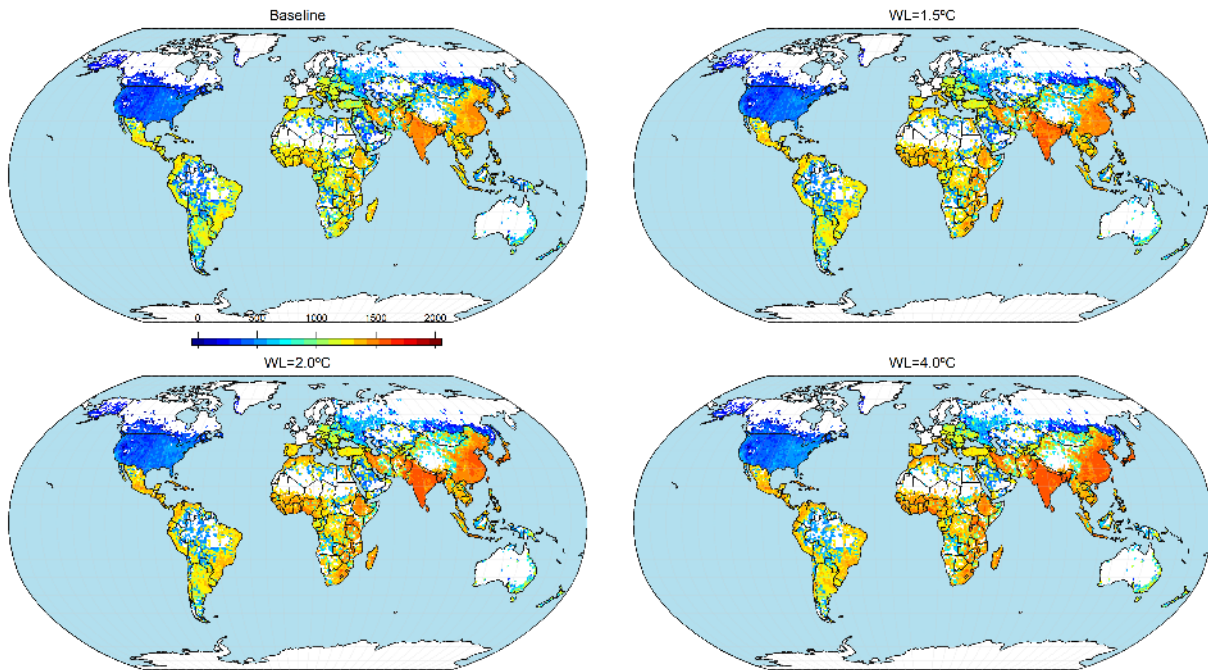


Figure 5.6. Total population affected by droughts for the present (baseline) and the specific warming levels (1.5°C, 2.0°C, 4.0°C) according to seven different climate models and RCP8.5 scenario. Country persons affected are disaggregated according to gridded population values. All estimates are using current population levels.

6.4 Summary

Results indicate that, under high end climate scenarios, droughts will become more frequent and severe at all specific warming levels considered. Their impacts could be devastating for the most vulnerable societies. Severe drought events that are rare in the present are projected to become frequent at warming levels larger than 2°C. Associated damage could increase up to tenfold in most vulnerable and populated areas, especially in Africa, Central and South America, and East Asia.

A framework to estimate global drought losses and population affected based on possible levels of warming is presented taking into account changes in climate and socio-economic dynamics. By means of an extreme value analysis, severity and recurrence of droughts were assessed over time slices centered on the years when specific warming levels of 1.5, 2.0, and 4.0 degree Celsius are exceeded.

This results shows the urgency to develop new and adjust actual adaptation and mitigation plans to reduce the effects of droughts and their links with water scarcity and desertification in areas that are actually at risk.

6. Water availability

6.1 Impact model used and methodology

JULES (Joint UK Land Environment Simulator) is a physically based community land surface model, comprised of the following modules: surface exchange of energy fluxes, snow cover, surface hydrology, soil moisture and temperature, plant physiology, soil carbon and vegetation dynamics (Best et al. 2011), with the latter being disabled for this application. The meteorological forcing data required for running JULES are: downward shortwave and long-wave radiation, precipitation rate, air temperature, wind-speed, air pressure and specific humidity (Best et al. 2011).

In JULES, each grid box is represented with a number of surface types, each one represented by a tile. JULES recognizes nine surface types (Best et al., 2011), five of which are vegetation surface types (broadleaf trees, needle leaf trees, C3 (temperate) grasses, C4 (tropical) grasses and shrubs) and four are non-vegetated surface types (urban, inland water, bare soil and ice). A full energy balance equation including constituents of radiation, sensible heat, latent heat, canopy heat and ground surface heat fluxes is calculated separately for each tile and the average energy balance for the grid box is found by weighting the values from each tile (Pryor et al. 2012).

In JULES the default soil configuration consists of four soil layers of thicknesses 0.1 m, 0.25 m, 0.65 m and 2.0 m. The fluxes of soil moisture between each soil layer are described by Darcy's law and a form of Richards' equation (Richards 1931) governs the soil hydrology. Runoff production is governed by two processes: infiltration excess surface runoff and drainage through the bottom of the soil column, a process calculated as a Darcian flux assuming zero gradient of matric potential (Best et al. 2011). Calculation of potential evaporation follows the Penman-Monteith approach (Penman, 1948). Water held at the plant canopy evaporates at the potential rate while restrictions of canopy resistance and soil moisture are applied for the simulation of evaporation from soil and plant transpiration from potential evaporation.

The forcing datasets used for this study are an ensemble of global high resolution climate model simulations, generated with the use of two GCMs (EC-Earth and HadGEM) in Atmospheric General Circulation Model (AGCM) mode. EC-Earth and HadGEM were run with prescribed sea surface temperature (SST), provided by different CMIP5 models. As a result, the generated simulations exhibit similar patterns of climate change to those of the driving CMIP5 models. Climate simulations that were available within HELIX but did not reach the higher level of examined warming (+4 °C) until the end of the simulation period (2100), were excluded from this analysis.

Climate change impacts are examined as differences between the temporal mean states of a future time-slice, corresponding to a SWL, and the reference period. It is important to mention that the SWLs are defined with respect to the pre-industrial period while the reference period corresponds to the recent past. The reference (or baseline) period spans from 1981 to 2010. The future time-slices are 30-year periods, centering on the year that each SWL is exceeded.

An exception had to be made for two ensemble members (EC-Earth-R4 and EC-Earth-R7), for which the end of the SWL4 time-slice exceeds the end of the simulation period by four and two years respectively. Thus, the SWL4 time-slices for EC-Earth-R4 and EC-Earth-R7 are comprised of 26 and 28 years respectively.

6.2 Hydrological simulations

Transient hydrological simulations, starting from 1971 and finishing at 2100, were performed with the JULES model driven by forcing data of each of the nine ensemble members. Ten spin up cycles of one year were performed to warm up the model before the beginning of the simulation period. JULES was run at the global scale (excluding Antarctica), with a spatial resolution of 0.5 x 0.5 degrees. The time step employed for the model runs was 1- hour.

6.3 Hydrological indicators

A number of hydrologic indicators are calculated from the runoff output of the JULES model, in order to express different aspects of runoff's temporal distribution. The employed hydrologic indicators are:

Mean runoff (RF mean): The long-term average of runoff is a basic indicator for mean water availability.

10th percentile runoff (RF low): The lower 10th percentile of runoff distribution serves as an indicator for low flows.

95th percentile runoff (RF high): The 95th percentile of runoff distribution serves as an indicator for high flows.

The hydrologic indicators are derived for each time-slice. Using the reference time-slice as a baseline for comparison, their changes at different levels of warming are examined both globally and locally. Local scale assessment is done at the hydrological basin level, for 21 major basins (shown in Figure) of different hydro-climatic regimes.

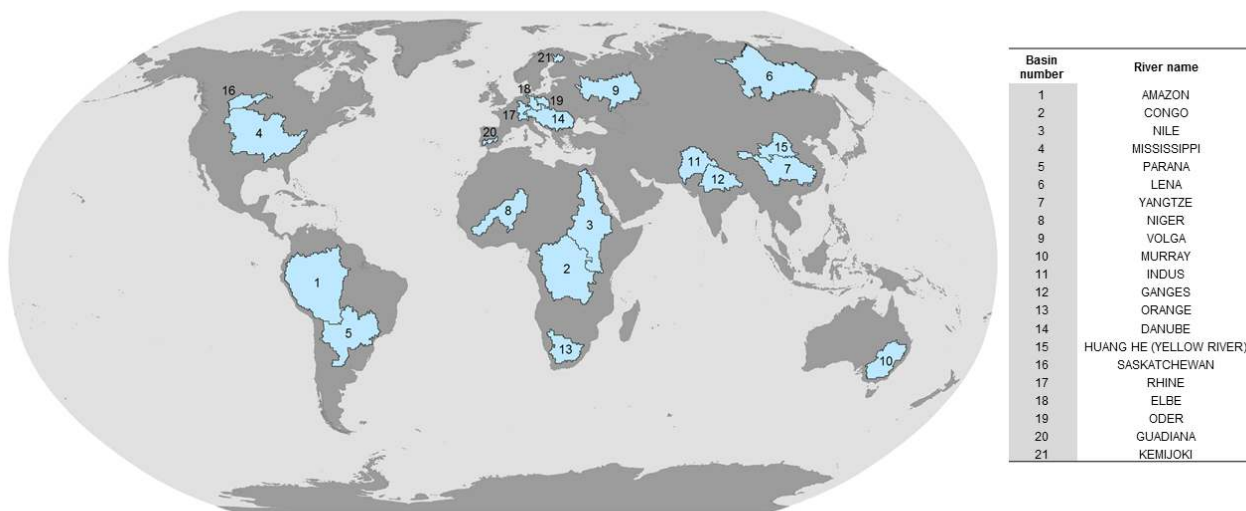


Figure 6.1. Examined hydrological basins, ranked in descending order according to their area.

6.4 Results - Global scale

Figure .2 shows the ensemble mean of percent changes in mean runoff per SWL and the associated model agreement. Mean runoff is projected to increase for the majority of the land surface, with the increase intensifying for higher SWLs. Regions with decreased projected mean runoff, especially at SWL4, are the Mediterranean, north Africa, central America and parts of south America. Model agreement is high (80 to 100%) for both the positive and negative changes in mean runoff.

The projected changes in low runoff per SWL are shown in Figure 6.3. The areas where low runoff of the baseline period is zero have been masked out (shown with white colour) in the maps of the changes and model agreement. Increases in low runoff are projected for the northern latitudes while mixed patterns are shown for the rest of the land surface. Reductions in low runoff with 80% to 100% agreement of the models are projected for the Mediterranean, northern and southern Africa, the Indian Peninsula, Australia, central America as well as parts of south America.

The ensemble mean changes projected for high runoff are depicted in Figure 6.4. According to the results, high runoff is expected to increase for the majority of the land surface. The projected increase in high runoff is more pronounced and the respective model agreement higher for SWL4. A few regions with projected decreases in high

runoff are encountered at the northern latitudes. In these regions the projected changes are possibly related to changes in snow accumulation and time of snowmelt.

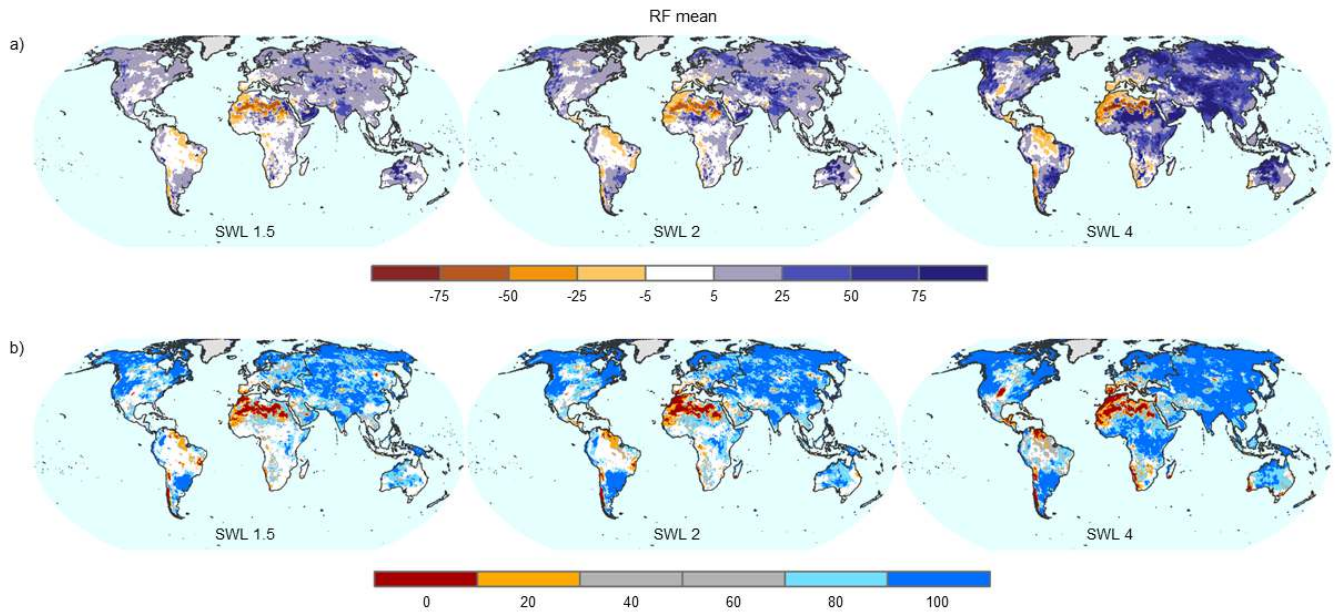


Figure 6.2. Percent change (%) in mean runoff per SWL compared to the baseline period: a) Ensemble mean change (%) and b) respective model agreement (%) towards an increase in mean runoff in the projected time-slices. Regions where relative changes are between -5% and 5% are masked out of the agreement representation (shown with white).

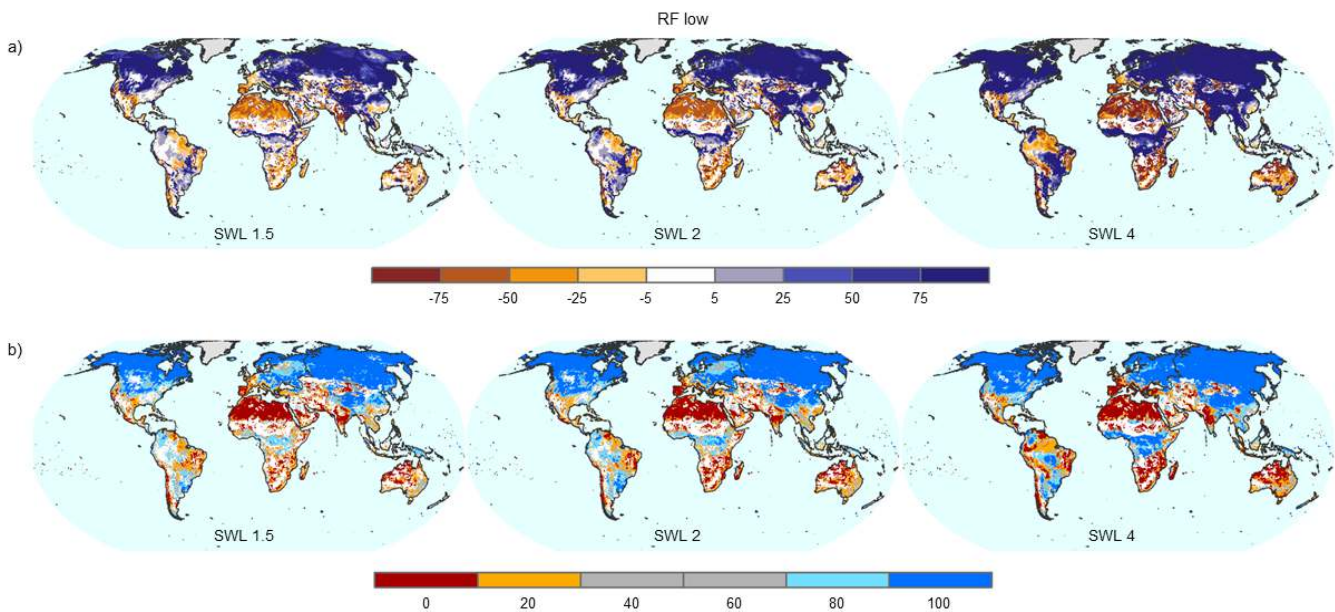


Figure 6.3. As Figure 6.2, for 10th percentile runoff (low runoff).

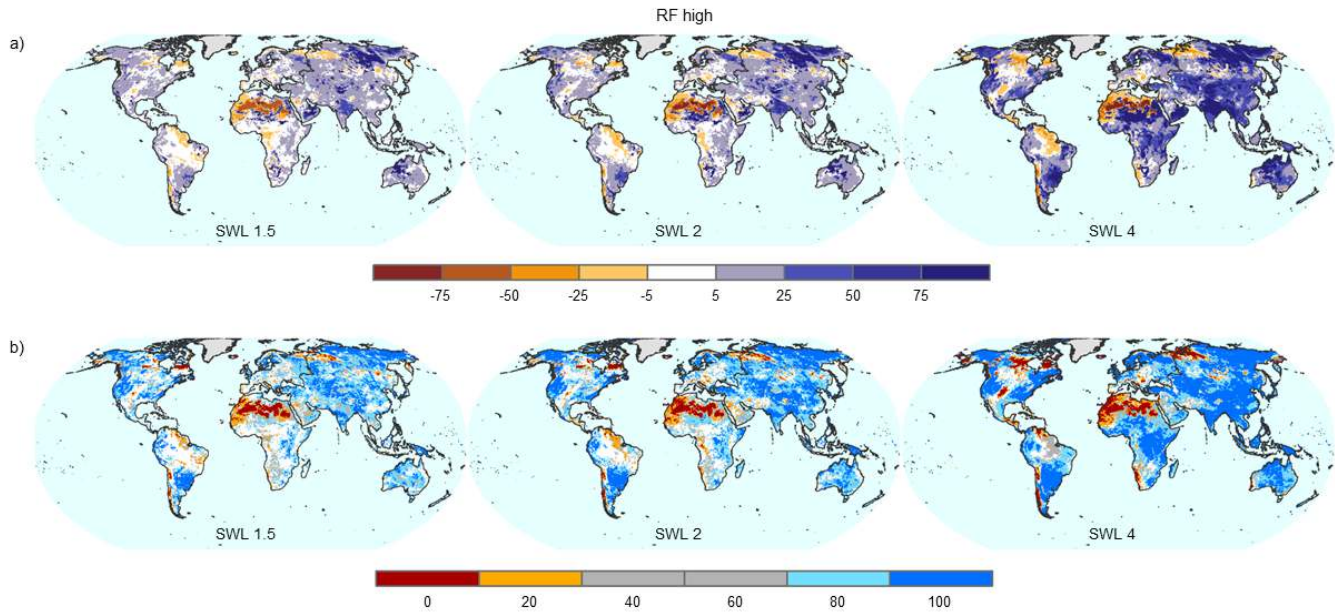


Figure 6.4. As Figure .2, for 95th percentile runoff (high runoff).

6.5 Basin scale results

Changes in basin aggregated mean and low runoff per SWL for the basins of study are shown in Figure 6.5 and 6.6 respectively. Increases in mean runoff are projected for the majority (19 out of the 21) of the basins. The two basins with projected decreases in mean runoff are both located in Europe (Danube and Guadiana). For most of the basins, the range of the ensemble members increases at SWL4 compared to the lower levels of warming.

Low runoff is also projected to increase for the majority of the examined basins and especially for those located in the northern latitudes. Projected decreases in low runoff are found for 4 basins. The largest decreases concern the Guadiana basin, located in the Mediterranean region that has been identified as a hotspot for negative changes in mean and low runoff from the global maps in Figure .2 and Figure . The range of the ensemble members at SWL is remarkably reduced, highlighting the agreement of the models towards low runoff decrease in this basin. A decreasing signal in low runoff is found for Amazon, which intensifies at higher warming levels. Negative signals for low runoff are also encountered in the Orange and Murray basins. For some basins, particularly the largest ones, the projected changes are small because there are regions of both positive and negative signals in the domain of the basin.

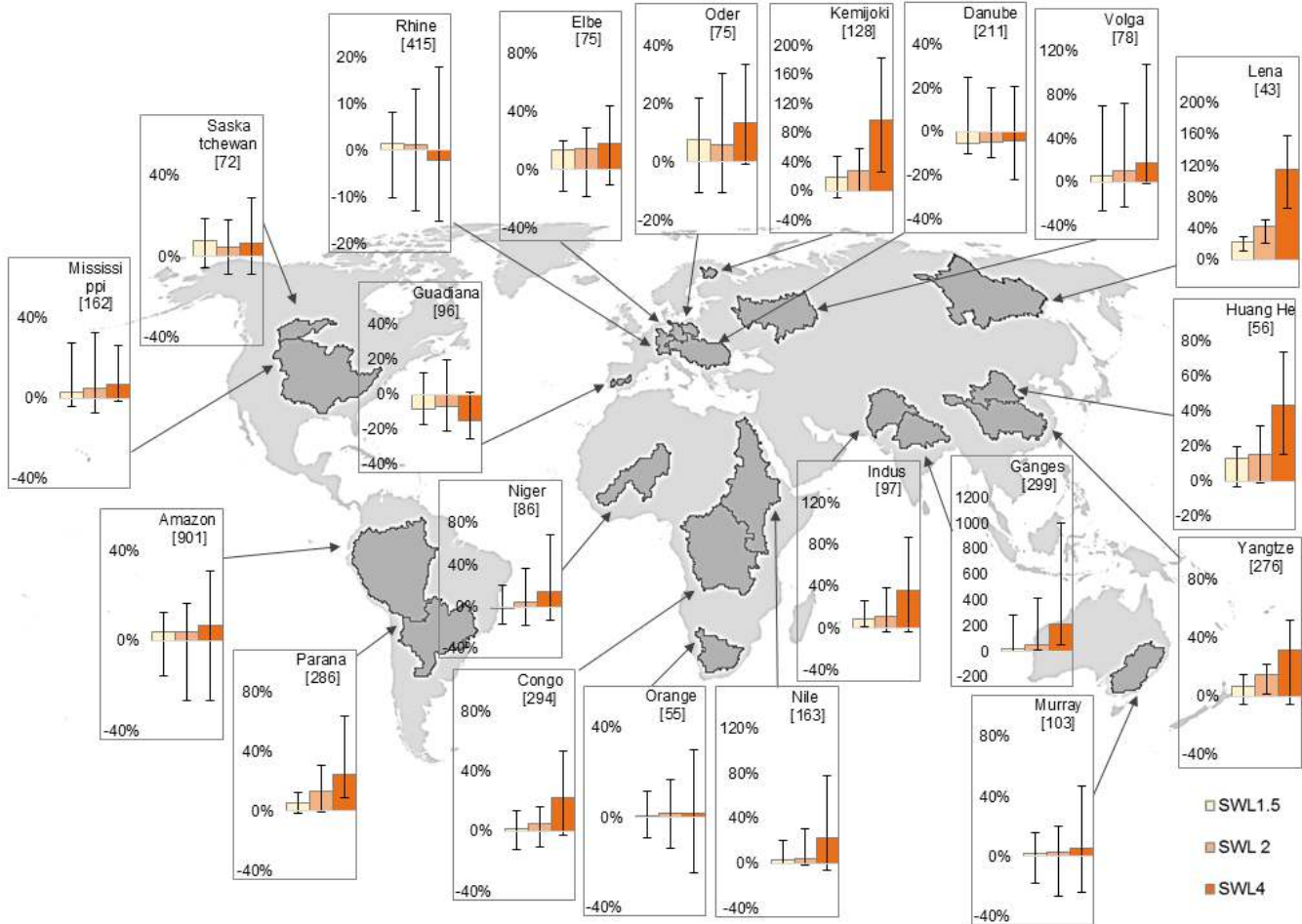


Figure 6.5. Changes in basin aggregated mean runoff per SWL compared to the baseline period. Column bars show the ensemble median changes and the error bars the range of the ensemble members. The number in brackets [] corresponds to the basin aggregated mean runoff of the baseline period in mm/year. Changes are shown as percentages (%). For the basins that changes exceed 200% the absolute differences (in mm/year) are shown instead.

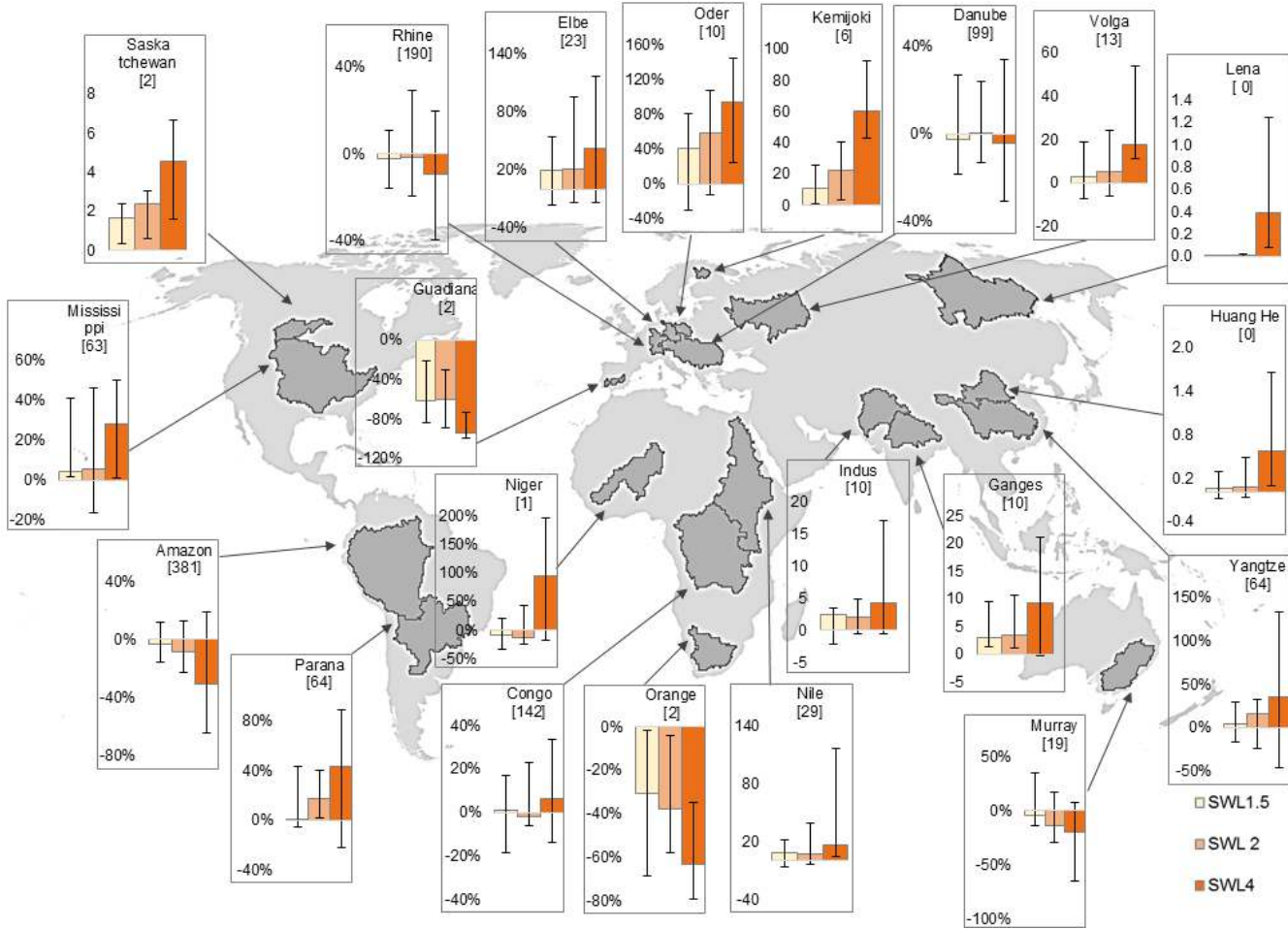


Figure 6.6. As Figure , for low runoff.

7. River flood risk

7.1 Introduction

Globally, almost one billion people live in floodplains (Di Baldassarre et al., 2013). Close access to fresh water resources provides drinkable water, fertile lands, protection barriers and navigable corridors. Yet, it increases the exposure to river flooding caused by extreme weather events. Societies have always strived to minimize the impacts of floods by reducing their vulnerability through a variety of flood mitigation measures including physical barriers, retention basins and early warning systems, among others (ABI, 2003; Alfieri et al., 2016b; Woodward et al., 2011). Since the early years of human settlements, actions to reduce vulnerability commonly occurred only after catastrophic events have hit (Kreibich and Thielen, 2009; Wind et al., 1999; Zurich, 2014). Yet, the intensification of the hydrological cycle due to global warming and increasing exposure raise growing concerns on future floods and their impacts on economy and health.

At the 21st Conference of the Parties (COP21) held in Paris in 2015, 195 countries joined forces to produce the first-ever global and legally binding climate agreement. The agreement aims to strengthen the global response to the threat of climate change (UNFCCC, 2015). Key point of the agreement is a joint effort to keep the increase in the global average temperature to well below 2°C above pre-industrial levels and to pursue efforts to limit the temperature increase to 1.5°C. Those goals appear in contrast with the latest observed trends recording global warming in the range of 1°C (GISTEMP Team, 2016; JMA, 2016) and a relentless increase towards the target levels. Scientists are now, more than ever, urged to investigate and quantify the socio-economic impacts of natural hazards under different degrees of global warming. Realistic impact estimates with the related uncertainty are key to inform international organizations, governments, reinsurance companies, and the IPCC, to support climate policy making, disaster risk reduction, and international agreements on climate mitigation.

Recent works in the field of global flood risk assessment have estimated the global population (Arnell and Gosling, 2014; Hirabayashi et al., 2013) and GDP (Jongman et al., 2012; Ward et al., 2014; Winsemius et al., 2013, 2016) exposed to river flooding in the present climate and under future climatic changes. Yet, key impact indicators such as direct and indirect flood losses have not been explicitly estimated so far in global scale analyses. Moreover, available estimates of people and assets exposed often rely on simplifications and assumptions needed to enable a global scale assessment including regions where data is scarce or unavailable. Novel research efforts have pushed forward the understanding and the mapping of global flood hazard (Dottori et al., 2016; Sampson et al., 2015), exposure (Freire et al., 2015) and vulnerability (Huizinga and De Moel, 2016; Scussolini et al., 2016), finally enabling process-based modeling of river flood risk at global scale under present and future climate conditions.

In this research we developed and applied a framework for global flood risk assessment based on a meteorological modeling chain coupled with state of the art maps of flood depth, exposure and vulnerability. We used climatic projections from seven downscaled General Circulation Models (GCMs) to estimate changes in the expected damage and population affected by river floods under Specific Warming Levels (SWLs) of 1.5°C, 2°C, and 4°C as compared to pre-industrial levels. Results are aggregated by country, river basin, continent, and global land surface, while the agreement of the ensemble projections is assessed through dedicated statistics.

7.2 Data

Key input to the flood risk assessment is the meteorological forcing data for the present and future climate. We used a set of seven climate projections with high concentration scenario (i.e., RCP 8.5) produced with EC-EARTH3-HR v3.1 (Alfieri et al., 2016a; Hazeleger et al., 2012) by the Swedish Meteorological and Hydrological Institute (SMHI). Projections are obtained by forcing EC-EARTH3-HR with Sea Surface Temperature (SST) and sea-ice concentration from independent driving GCMs produced within the Coupled Model Intercomparison Project Phase 5 (CMIP5) as

described in the introduction. The benefits of downscaling the original models output with EC-EARTH3-HR are to increase and level out the spatial resolution, from their original grids – different for each forcing model – to 0.35° , leading to an improved characterization of extreme events and comparable statistics among different models.

To define inundation depth and extent for simulated river flood events we make use of the global flood hazard maps developed by Dottori et al. (2016) for six return periods between 10 and 500 years under present climate conditions. Maps were produced at 30 arc-second resolution (~ 1 km at the equator) with a two-dimensional hydrodynamic model designed to ensure an accurate representation of flow processes in the river network and in the flood plains. Dottori et al. (2016) and Alfieri et al. (2013) assessed the performance of the flood hazard maps and of their underlying global streamflow climatology, considering several river basins, flood events and more than 600 river gauges across the globe.

Population data was taken from the Global Human Settlement Layer (GHSL) Global Population Grids (Freire et al., 2015; Pesaresi et al., 2013). It includes estimates for the year 2015 and it was derived by upscaling the original product at 250 m resolution, to 30 arc second resolution.

Further datasets used in the risk assessment include the FLOPROS (Scussolini et al., 2016) global database of FLOod PROtection Standards; land use from the GlobCover 2009 (Bontemps et al., 2011); and damage functions by Huizinga and de Moel (2016). The latter define the relation between inundation depth and the corresponding direct economic damage per unit surface. Damage functions are defined per sector, including residential, commercial, industrial, infrastructures and agriculture. Country-specific functions per sector have been derived by multiplying the maximum unit damage per country by linear step-functions defined at continent level (see Huizinga and De Moel, 2016).

7.3 Methods

In this work, all hydrological variables are modeled through three levels of grid resolution, so to optimize the tradeoff between information content and computing resources needed (Figure 7.1):

- 1) A global hydrological model was set up at 0.5° resolution (~ 55 km at the equator) to run 130+ years of daily climatic projections for seven independent models, and estimate changes in flood magnitude and flood frequency under climate change.
- 2) A streamflow climatology was produced with a global hydrological model run in transient mode over 34 years at daily temporal resolution (Alfieri et al., 2013). Spatial resolution used is 0.1° (~ 11 km at the equator).
- 3) Flood hazard maps at 30 arc second (~ 1 km at the equator) were derived from the global streamflow climatology for six selected return periods. Details on methods and output are given by Dottori et al. (2016).

The proposed framework for global flood risk assessment is based on two key components: 1) estimation of the potential impacts of flood events with magnitude corresponding to the 6 selected return periods under present climatic conditions, and 2) estimation of the magnitude and frequency of extreme flood events in the present and future climate. Those are described in the following sections.

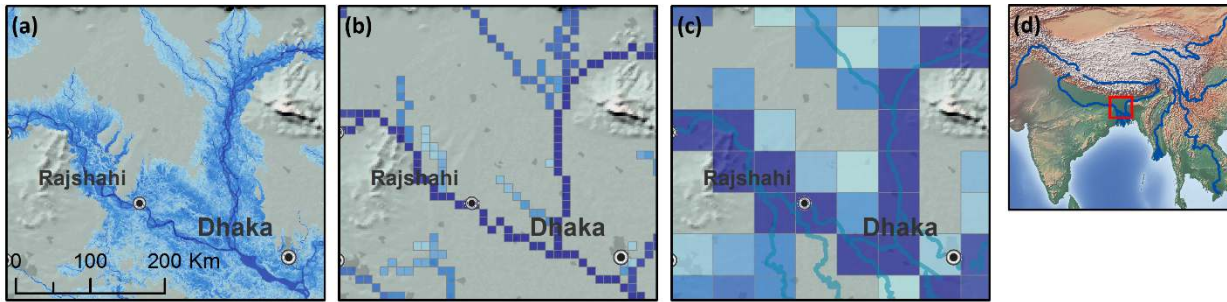


Figure 7.1: The three levels of spatial resolution used - illustrative example for the Ganges-Brahmaputra confluence. Shades of blue are proportional to flood depth (a), river discharge (b), and upstream area (c).

Potential flood impacts

We derived maps of potential population affected and potential damage for six flood return periods ($T_F=10, 20, 50, 100, 200$ and 500 years) under present climatic conditions. Impact maps at 30 arc second resolution are obtained by combining global flood hazard maps by Dottori et al. (2016) with exposure data in the form of population density and land use, and with vulnerability information expressed by the flood damage functions. Potential population affected are estimated by overlaying population density and flood hazard maps, assuming population to be affected for any positive flood depth. Potential damage maps are generated for each of the five sectors by combining inundation depth with the damage functions and with maps of percent land use pertaining to each sector, derived from the GlobCover at 10 second (~ 300 m) resolution. Maps of potential impact were aggregated at the resolution of the hydro-climatic forcing of 0.5° using a physically-based approach proposed by Alfieri et al. (2015), which assigns flooded areas to the grid point of the causative inflow hydrograph at coarser resolution. In this case, flood polygons were first aggregated at 0.1° resolution of the flood hydrographs and then upscaled to 0.5° according to the drainage direction.

Climatic projections of the frequency and magnitude of river floods

Daily streamflow simulations at 0.5° resolution were produced with the Lisflood model (Alfieri et al., 2016a; Burek et al., 2013; van der Knijff et al., 2010) forced by seven climatic projections starting in 1971, using temperature, precipitation and potential evapo-transpiration as input variables. The latter was estimated using the Penman-Monteith equation calculated with daily mean temperature, wind speed, relative humidity and solar radiation as input. For each grid cell and climate projection, we fitted a Gumbel extreme value distribution on the series of 30 discharge annual maxima between 1976 and 2005, with the method of L-moments (Hosking, 1990). Significance of the analytical curves was assessed by bootstrapping, using 1,000 repetitions for each fit. A Peak Over Threshold (POT) routine was used to select flood events simulated in the present and future climate. To this end, we first calculated the return period of simulated discharges for the available time windows by inverting the analytical Gumbel distributions. High flow events above natural bank full conditions are defined as the set of contiguous discharge values with return period larger than 2 years (e.g., Carpenter et al., 1999). Then, high flow events with maximum return period larger than the local value of flood protections are considered as flood. Note that the output of such analysis is not the quantitative streamflow estimation, but rather the timing and magnitude of simulated flood events. Hence, the use of the raw model output in place of bias corrected alternatives is a suitable option for the impact assessment. On the other hand, this avoids a number of issues affecting bias corrected climate scenarios, namely, 1) breaking the physical links between the atmospheric variables; 2) strong influence of the quality and resolution of the observational dataset on the output product; 3) bias corrected datasets are often associated with a decrease in model resolution; 4) questionable benefits of the bias correction for extreme events (Ehret et al., 2012; Huang et al., 2014; Muerth et al., 2013; Themeßl et al., 2012).

Projections of flood risk at specific warming levels

The socio-economic impact of river floods in the present and future climate is assessed by linking every simulated flood event to its potential damage and population affected, by applying linear interpolation between the six modeled return periods (see Sect. 7.2). Results are aggregated over four time horizons of 30 years each: a baseline scenario between 1976 and 2005, and three future scenarios centered on the year of exceeding the three SWLs of 1.5°C, 2°C, and 4°C for each of the seven models. Given the inherent low frequency of flood events, impact values simulated for each grid cell are aggregated at different spatial levels to increase their robustness. Spatial aggregations were performed by country, continent (Russia was considered as a separate continent, being the world's largest trans-continental country), global land surface and large river basins with area in excess of 500,000 km² (Figure). The agreement of country aggregated estimates from an ensemble of seven climatic projections is assessed with the Student's t-test on the projected changes in impact between the baseline and each SWL.

This research aims to explore changes in flood risk at different warming levels, independently from when those occur. Hence, we did not include the effect of socio-economic changes such as projections of population, Gross Domestic Products (GDP), or land use. Impact estimates refer to population estimates of 2015 and damage in EUR at Purchasing Power Parity (PPP) in 2010 values.

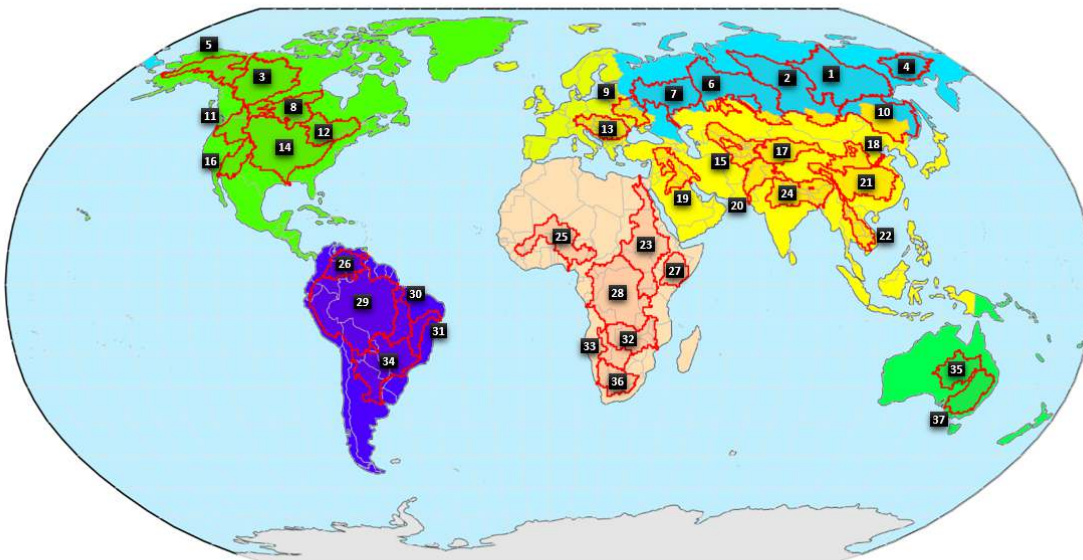


Figure 7.2: Map of continents (in colors) and river basins (red contours) considered in the study. River basins are 1 - Lena, 2 - Yenisey, 3 - Mackenzie, 4 - Kolyma, 5 - Yukon, 6 - Ob, 7 - Volga, 8 - Nelson, 9 - Dniepr, 10 - Amur, 11 - Columbia, 12 - St. Lawrence, 13 - Danube, 14 - Mississippi, 15 - Lake Aral, 16 - Colorado, 17 - Tarim, 18 - Huang He, 19 - Tigris and Euphrates, 20 - Indus, 21 - Yangtze, 22 - Mekong, 23 - Nile, 24 - Ganges and Brahmaputra, 25 - Niger, 26 - Orinoco, 27 - Juba-Shebelle, 28 - Congo, 29 - Amazon, 30 - Tocantins, 31 - Sao Francisco, 32 - Zambezi, 33 - Okavango, 34 - Parana, 35 - Eyre Lake, 36 - Orange, 37 - Murray – Darling.

7.4 Results

Trend in precipitation extremes

We analyzed trends of extreme annual precipitation cumulated over durations of 1, 5 and 10 days, in 37 large river basins. Those are useful non-parametric indicators complementing the assessment of the future flood hazard. Climate projections point towards an intensification of the hydrological cycle, with the vast majority of river basins projected to experience more extreme precipitation events over durations typically associated with large scale floods. The average trend of the ensemble was assessed through linear regression while the statistical significance was tested with the Mann-Kendall statistics for monotonic trends (Kendall, 1975; Mann, 1945). Results are shown in

Figure 5.3 for three river basins and for the World's land surface, while data for 34 more river basins can be found in Alfieri et al. (2016a). An increasing trend of maximum daily precipitation is projected for all river basins, with significance level exceeding 95% (i.e., $p_{MK} < 0.05$) in all cases except that of the Okavango. Over longer accumulations trends remain mostly positive despite becoming weaker in arid regions. Trends of 10-day maxima are significantly increasing for 32 out of 37 basins, unchanged for the Colorado and the Australian's Murray-Darling and Eyre Lake, and significantly decreasing in the Okavango and Orange, in Southern Africa. Under high-end climate change, projections for the entire land surface indicate *virtually certain* ($\sim 100\%$ confidence) increase of annual precipitation maxima, with average rates between 0.13 (1-day) and 0.24 (10-day) mm/year.

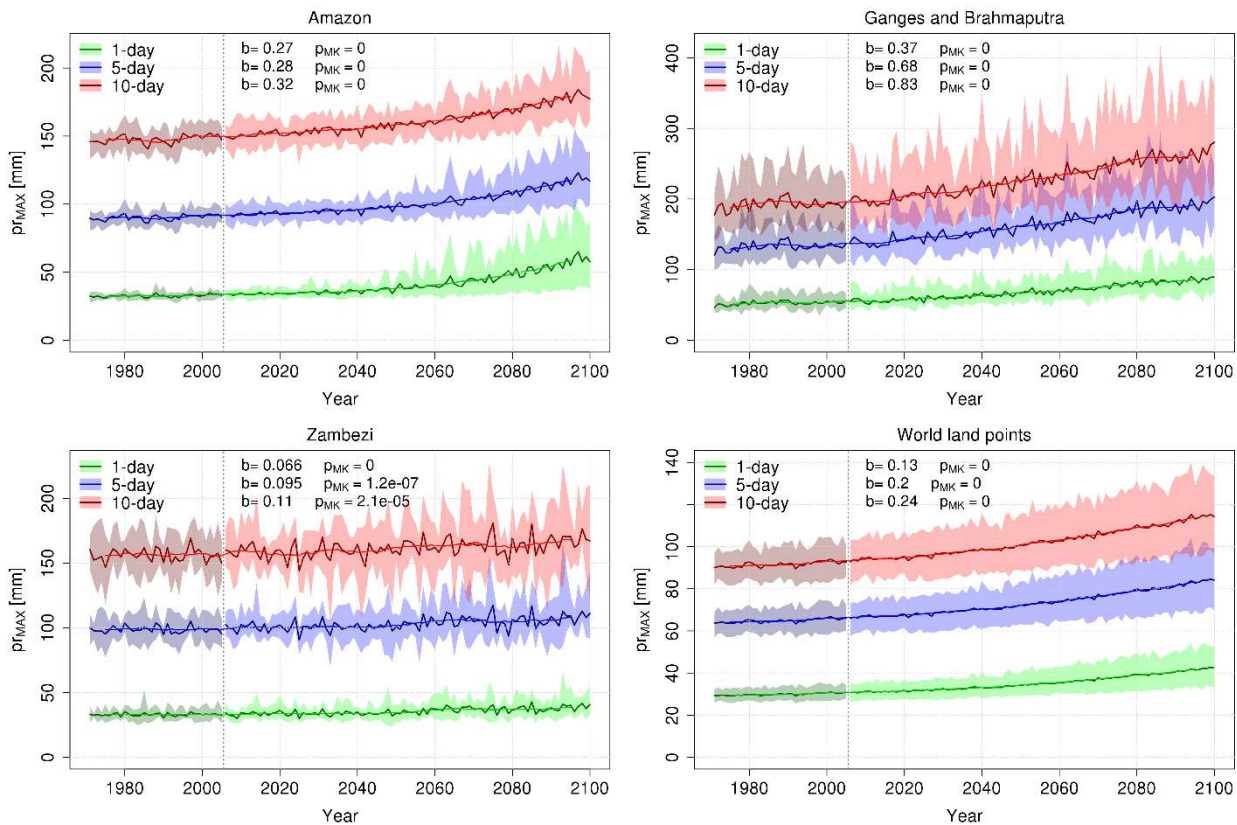


Figure 5.3: Multi-model ensemble projections of annual maximum precipitation over 1, 5, and 10 days. Three panels show zonal averages for the Amazon, Ganges and Brahmaputra, and Zambezi river basins. The fourth panel refers to all world land points except Antarctica. Statistics on each panel show the slope b of the linear regression (in mm/year) and the p -value for significance of the Mann-Kendall test for trend.

Flood statistics at SWLs

We analyzed the statistics of simulated flood events to detect significant changes in the flood hazard at SWLs. Figure compares the empirical recurrence interval of simulated events with their theoretical values as derived by the corresponding analytical distributions. Flood events are aggregated by continent and include all seven scenarios, so to increase the sample robustness and enable the analysis of extremely rare events in the order of 1 in 10,000 years. All floods peaks are transformed into their return periods using the analytical curves derived for the baseline scenario so that, in the ideal case, the grey lines would match the 1:1 line. However, lines tend to flatten for low theoretical return periods thanks to the effect of flood protections preventing floods to occur. Similarly, empirical lines tend to loose steepness for increasing return periods, due to the autocorrelation of the flood magnitude along the drainage network, as previously noted by Jongman et al. (2014) in a large-scale assessment.

Graphs indicate a significant increase in the frequency of extreme events for all SWLs. This appears as a decrease in the future recurrence interval of simulated floods with the same intensity as in the baseline. As an example, in Africa, events with a present theoretical return period of 100 years were simulated to occur on average every 185 years (95% confidence interval within 80 and 360 years). These figures are projected to drop to 1 in 40 years at 1.5°C and 2°C and 1 in 21 years at 4°C warming, implying that protection standards will need to be upgraded to ensure the same statistical level of protection. In North America, most regions are presently protected to the 1 in 100 year flood, though at 4°C warming these standards will only withstand up to the 1 in 10 year flood. On average, red lines indicating changes at 4°C lie well below those of milder warming levels for all continents except that for Europe, where similar changes are expected for all warming levels.

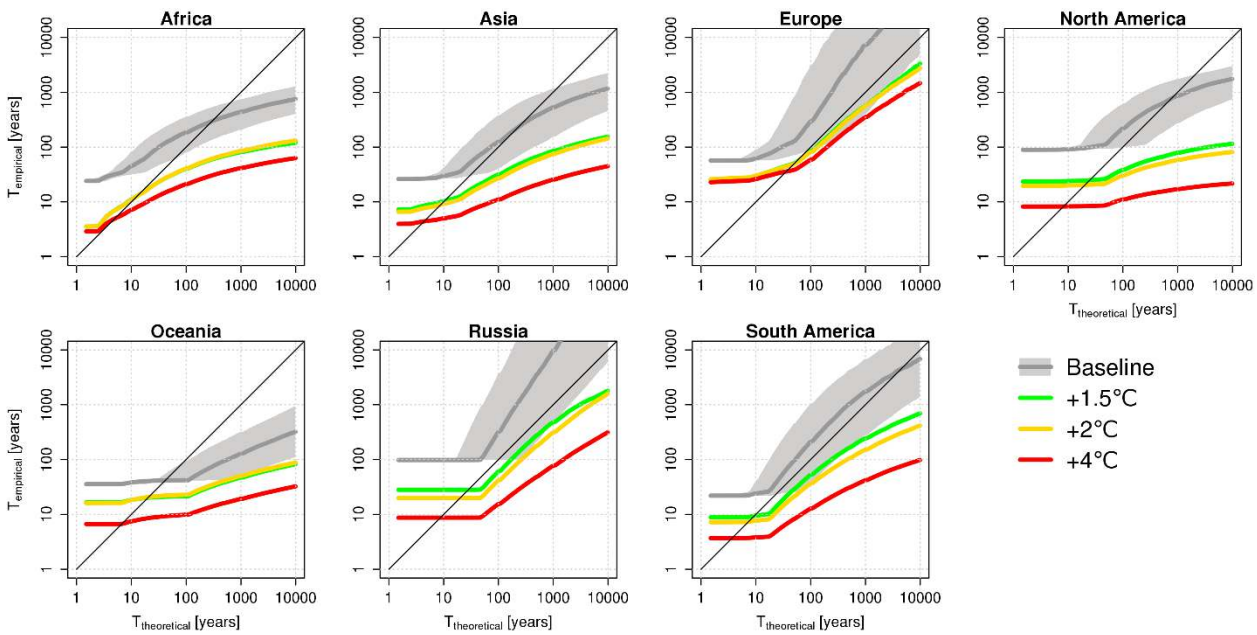


Figure 7.4: Empirical recurrence intervals, in years, of simulated flood events per continent in the baseline and at SWLs. 95% confidence bands are shown in grey for the baseline window.

Global projections of flood risk

Flood impact was derived for each simulated flood and then aggregated over different temporal and spatial scales to achieve robust statistics for the present and future climate. Annual ensemble projections of damage and population affected till 2100 are shown in Figure 7.5, while Table 7. shows the modeled flood impact in the baseline scenario (i.e., 1976-2005) disaggregated by continent and economic sector. Impact values simulated over past events cannot be compared directly with observed figures, as the historical scenario of climate projections does not reproduce the day-to-day history of the observed climate but rather a coherent evolution of the atmosphere under a specific climatic forcing. Yet, simulated scenarios reproduce skillfully the magnitude of the socio-economic impact of observed river floods over large spatial and temporal aggregations. Central estimates of global flood risk in the baseline scenario total 54 million people affected and 58 billion EUR (75 billion USD) of damage per year. Estimates of population affected compare well in magnitude with observed data, reporting 81 million (1975-2001) and 109 million (1995-2015) people per year (Jonkman, 2005; UNISDR and CRED, 2015). Larger uncertainty affects official figures on global flood losses, where reported 29 billion USD per year (1980-2014) (Munich Re, 2015) are in contrast with the supposedly more realistic estimates of 104 billion USD per year by the Global Assessment Report (UNISDR, 2015), the latter pointing out that only 35% of weather related disasters include information about economic losses.

Simulated impacts in the baseline are largest in Asia and Africa, which together account for 95% of people affected and 73% of the economic damage. The sector disaggregation shows that residential damages represent up to half of

the total losses, followed by commercial and industrial impacts. Agricultural damage often takes a minor proportion, though it reaches 13% in Africa and 7% in Asia and South America. The damage share by sector did not change significantly in the future scenarios (not shown), due to the assumption of constant land use and population density. Under a high-end climate scenario, global flood impacts are projected to rise at an average rate of 2.4 million people and 3 billion EUR per year, exceeding a four-fold increase in flood risk by the end of the century due to climate change only.

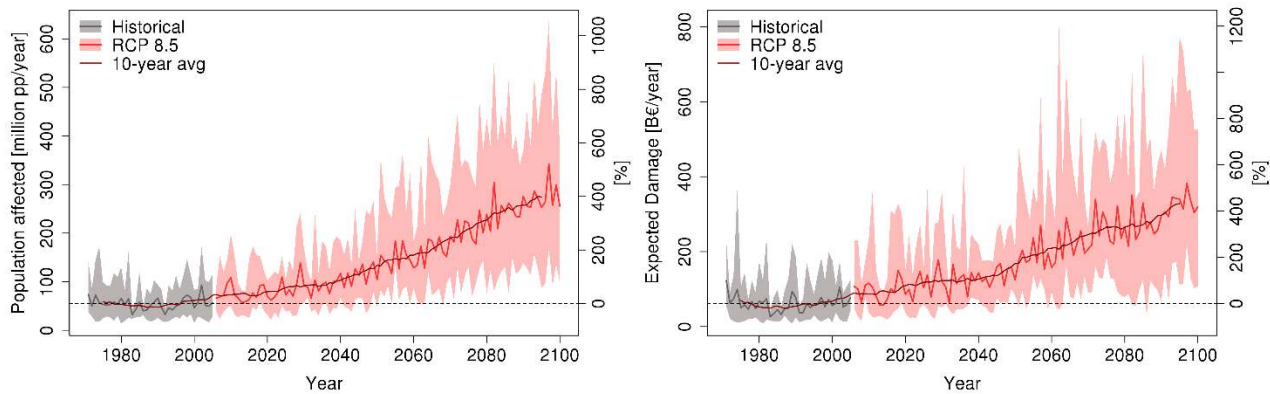


Figure 7.5: Projected population affected and expected damage per year and relative change from the baseline scenario. Multi-model mean, spread and 10-year running mean of world-wide aggregated figures.

Table 7.1: Modelled population affected and damage for each continent in the baseline scenario (ensemble mean), together with sector disaggregation of damage.

	Population Affected		Damage				
	[millions/year]	[B€/year]	Agriculture	Residential	Commercial	Infrastructure	Industrial
Africa	16.5	6.5	13%	36%	33%	0%	17%
Asia	35.0	35.9	7%	39%	32%	1%	21%
Europe	0.5	4.6	1%	45%	32%	1%	21%
North America	0.8	1.8	2%	46%	27%	6%	20%
Oceania	0.1	4.9	1%	48%	32%	0%	19%
Russia	0.2	3.2	1%	43%	34%	0%	22%
South America	1.1	1.5	7%	39%	31%	1%	22%

Future flood risk per country at SWLs

Maps of changes in flood impacts per country at 1.5°C, 2°C, and 4°C are shown in Figure 7.6. A confidence level of 90% is used to display the multi-model agreement. Following the IPCC terminology for likelihood (Mastrandrea et al., 2010), countries with no hatching in the figures are *very likely* to experience significant changes of flood risk. Changes in flood risk appear unevenly distributed, with the largest increases in Asia, America and Europe. On the other hand, projected changes are statistically not significant in most countries in Africa and Oceania for all considered warming levels. Relative changes in population affected (damage) at 4°C warming are projected to exceed 1000% in 15 (16) countries in Central Europe, South Asia, South America and Japan (confidence = 90%), as compared to 1976-2005.

Negative changes in flood risk are found in some countries in Europe and Africa, in agreement with the regional assessment on Europe by Alfieri et al. (2015). Interestingly, only Latvia showed statistically significant negative changes at all SWLs for both impact indicators.

Figure 7.7 shows the top 20 countries projected to be impacted the most by future floods, ranked by largest impacts at 4°C global warming. Countries 21 to 100 are shown in Alfieri et al. (2016a), together with a ranking by river basin. Largest absolute impacts are found in China, where current estimates of 9 million people affected and 25 billion EUR damage per year are projected to rise with the global warming, reaching 40 million and 110 billion EUR per year at 4°C warming. A remarkable finding is the more than 20-fold increase in flood risk in India and Bangladesh at 4°C warming, which puts them in the first 3 (8) countries by population affected (damage). Also, in spite of the relatively high standards of flood protections in the EU28 countries, projected increase in flood risk is estimated to place the European Union as a whole as third (fourth) most affected country by expected damage at 1.5°C and 2°C (4°C) warming.

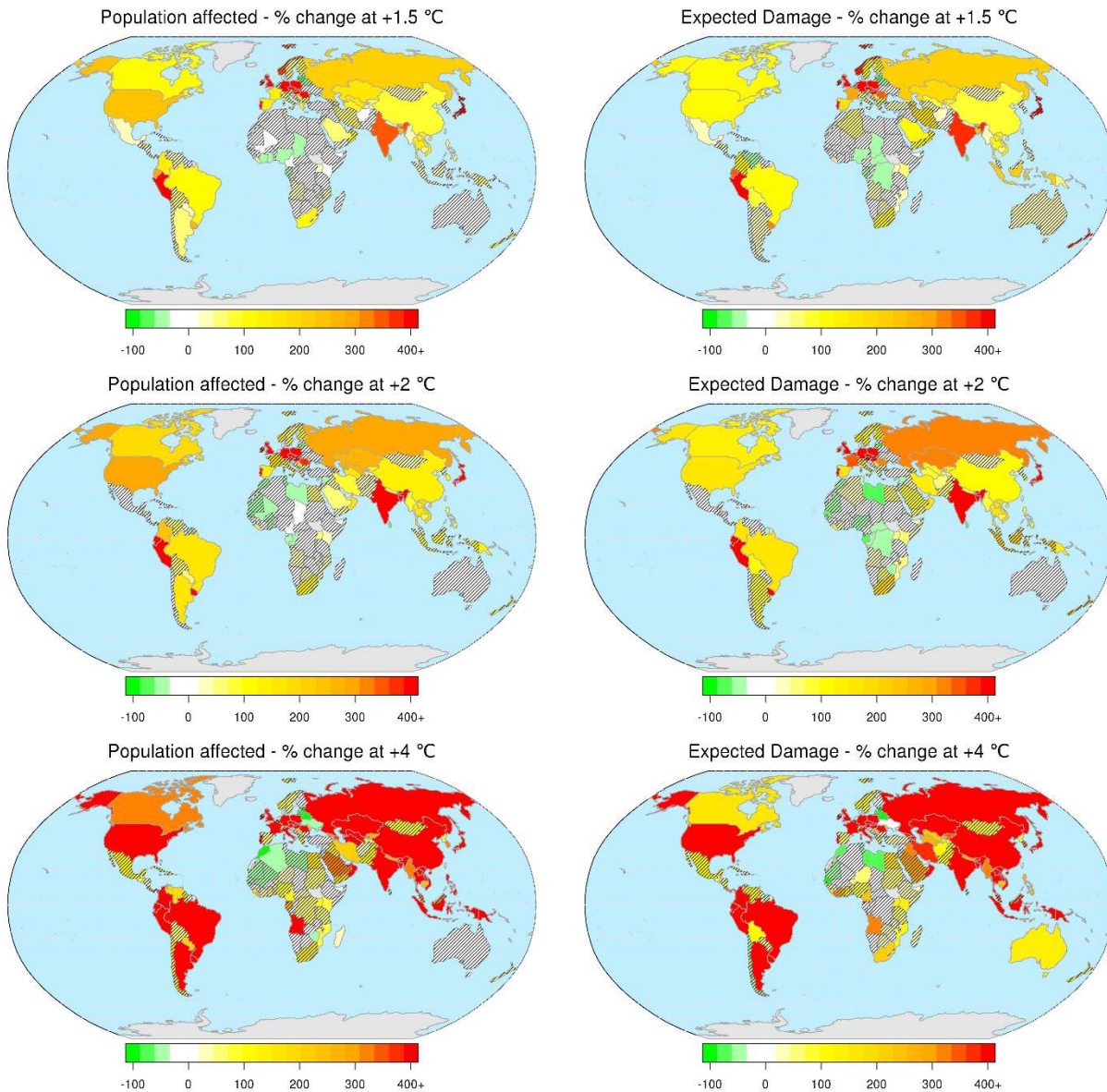


Figure 7.6: Average change in population affected (left) and expected damage (right) per country at SWLs. Hatching indicates countries where the confidence level of the average change is less than 90%.

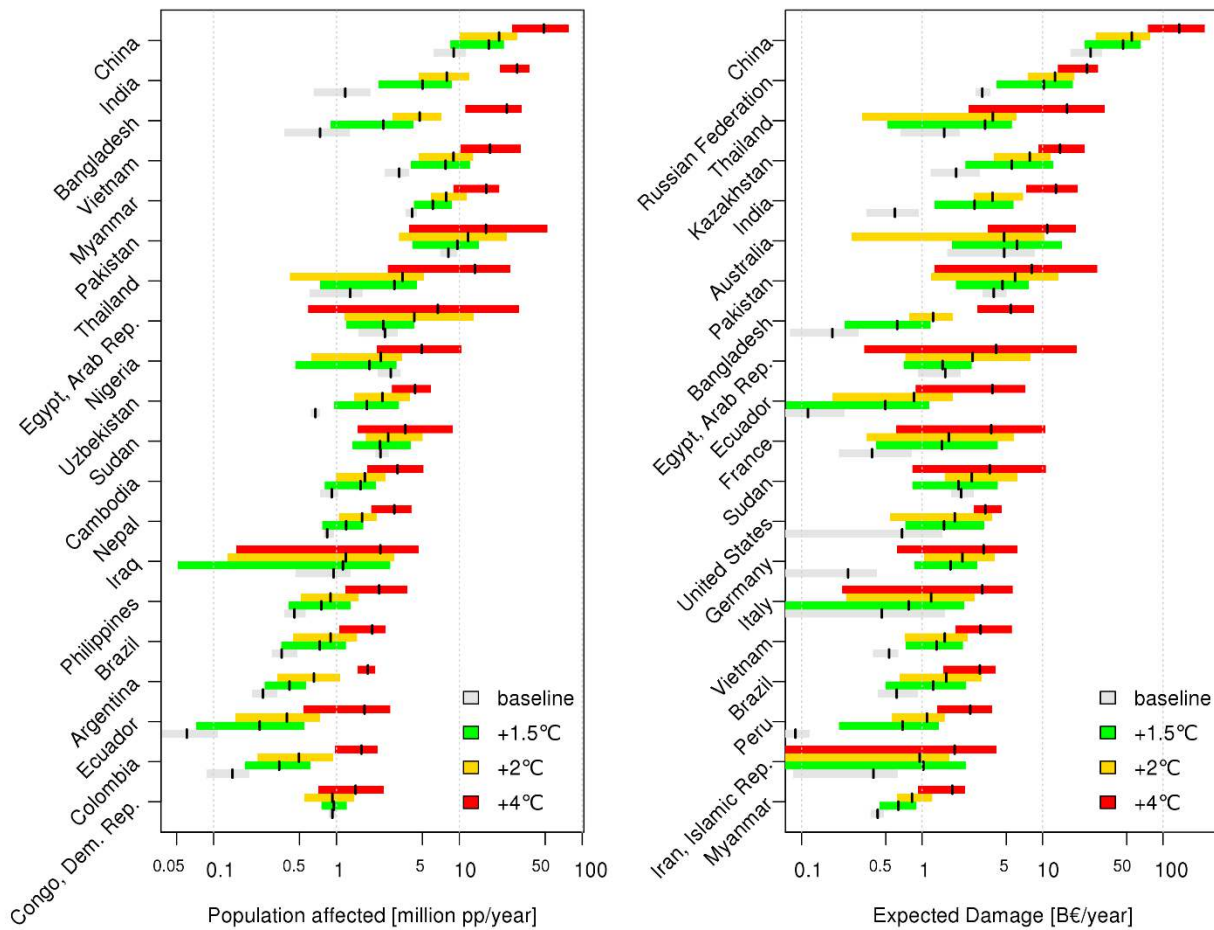


Figure 7.7 Population affected and expected damage in the baseline and at SWLs (mean value and ensemble spread). Top 20 countries ranked by largest impact at 4°C global warming.

7.5 Discussion and conclusions

This research presents a novel framework to explore the socio-economic impacts of a changing climate on the future flood risk at global scale. We used an ensemble of seven high-end climate scenarios as meteorological input and assessed the changes in flood risk under specific warming levels of 1.5°C, 2°C, and 4°C, considering different spatial aggregations including countries, continents, large river basins and global land areas.

The risk assessment framework provided skillful estimates of the global flood impact in the present climate, proving itself as a suitable tool for impact assessment under climate change. Results of this research clearly point out a positive correlation between global warming and global flood risk. Our analyses reveal that the intensification of the hydrological cycle caused by warmer air temperature is linked to more extreme rainfall accumulations in all world regions, particularly over short durations. Flood events with occurrence interval larger than the return period of present flood protections are projected to rise in all continents under all considered SWLs, leading to widespread increase in the flood hazard. Statistically significant increase in flood risk was found in most world regions due to the combination of the future flood hazard and information on global exposure and vulnerability. Our findings indicates that, at 4°C global warming, countries representing 73% of the world population and 79% of the global GDP will *very likely* experience increasing flood risk at an average 580% increase in population affected and 500% increase in damage, as compared to the impact simulated over the baseline period 1976-2005. Such figures reduce to 100%

(170%) increase in population affected and 120% (170%) increase in damage for a warming level of 1.5°C (2°C). Projected changes are not homogeneously distributed on the world land surface. Largest increase in flood risk was found in America, Asia and Europe while negative changes were found in only few countries in Eastern Europe and Africa. In contrast, the multi-model projections did not agree on a significant change in flood impacts in several countries in Africa, Oceania, Central America, Northern Europe and Middle East.

The model framework we used includes unprecedented features for global flood risk applications, which were possible thanks to recent progresses in global datasets on flood hazard, exposure and vulnerability. Key advances over previous works are:

An event-based selection of simulated flood peaks, enabling more accurate detection of nonlinear patterns of change in flood frequency and magnitude under non-stationary climate.

A multi-resolution approach, which maximizes the computing power in the representation of different variables and enables the coupling of large datasets. Key example is the use of high-resolution global flood hazard maps to estimate the impact of floods, coupled with 130+ year climatic projections at daily resolution to assess the flood frequency.

The first global-scale assessment of flood damage, rather than the commonly used exposed GDP, thanks to recent efforts in producing global flood damage functions (Huizinga and De Moel, 2016) and of the release of the first global dataset on flood protections (Scussolini et al., 2016). Similarly, advances in mapping the global population distribution (Pesaresi et al., 2013) has significantly increased the accuracy in the estimation of population affected by floods.

Findings and implications of this work should be evaluated by considering some underlying modeling assumptions. We assume that impact levels at SWLs are independent of the timing of the warming and of the pathways of the greenhouse gas concentrations. In the presented work, we evaluated impacts on 30-year windows centered on the year of passing each SWL, without considering longer term inertial effect under hypothetical stabilization scenarios corresponding to each SWL. We used RCP 8.5 projections as they normally exceed 4°C warming by the end of the current century, hence all three considered SWLs could be analyzed in the same set of simulations. Despite its limitations, this assumption is commonly accepted by the scientific community and adopted in a number of recent works (Hirabayashi et al., 2013; James and Washington, 2013; Koutroulis et al., 2016; Swain and Hayhoe, 2014). Also, this research focuses on impacts due to riverine flooding in river sections with upstream area larger than 5,000 km², consistently with the underlying inundation maps by Dottori et al. (2016). Impacts from flash floods, pluvial floods and coastal floods are not simulated by the impact model.

It is worth noting that, even under the very limited warming scenario of 1.5°C, we estimate a more than doubling of global flood risk as compared to 1976-2005. This implies that effective adaptation plans would be required if the aim is to keep flood risk rates within the current levels or below. In addition, socio-economic drivers are likely to make impacts higher in developing countries and in regions with significant population growth. The increase in flood risk may become unsustainable in regions where the combination of socio-economic and climatic drivers is particularly adverse.

8. General Conclusions

This deliverable presents initial results from the HELIX impact models, assessing the impact of different specific warming levels on several different natural and human systems. The general methodology adopted (with some inevitable minor deviations) is the following. Two HELIX high-resolution atmospheric only climate models, EC-Earth and HadGEM3 were used here. Both models were driven by the RCP8.5 scenario (greenhouse gases forcing) as well as by prescribed sea surface temperature (SSTs) coming from a range of CMIP5 climate simulations. A total of 9 high resolution climate forcing were made available to the impact modelling groups. All climate forcing were then bias corrected using the Princeton Princeton v2 hybrid dataset of observed climate variables (Sheffield et al., 2006). Doing this ensured that impact models were rooted in present-day climate, i.e. changes in the future are relative to actual present-day baseline. All impact models used a common baseline, the average over 1981-2010. For most impact estimates, the impact of warming was quantified for 3 different warming levels, 1.5°C, 2°C and 4°C above pre-industrial level. Climate change impacts were quantified for systems including biomes, biodiversity, crop yield, water availability and runoff, global droughts and damages on population and economy, and river floods and damages on population.

The initial results show for all systems increasing level of impact with increasing warming levels. Some preliminary conclusions are summarised here:

- River floods are projected to increase with warming levels, with worldwide increase for 4°C warming.
- Runoff is projected to increase in mid-latitudes but decreases in the tropics, with non-linear response to warming levels. Increase in atmospheric CO₂ contributes to the runoff increase via the CO₂ impact on stomatal conductance and plant evaporation.
- Drought severity is projected to increase in most region of the globe (apart from Northern hemisphere Eurasian continent), with economic damage increasing exponentially with warming levels.
- Biomes show a general increase in productivity and carbon stored in the future driven by the increase in atmospheric CO₂. This increase is larger than the potential climate induce decrease in productivity.
- Forest cover increases in mid and high latitudes of the Northern hemisphere but declines in several tropical regions
- Crop yields (particularly rice, maize and wheat) show a strong decrease at 4°C warming in response to changes in mean climate, although neither CO₂ fertilization nor effects of changing weather extremes have yet been examined for crops.
- Biodiversity loss increase substantially between 2 and 4°C (more than a doubling), suggesting a potential tipping point.

9. References

- ABI: Assessment of the cost and effect on future claims of installing flood damage resistant measures, 2003.
- Alfieri, L., Burek, P., Dutra, E., Krzeminski, B., Muraro, D., Thielen, J. and Pappenberger, F.: GloFAS – global ensemble streamflow forecasting and flood early warning, *Hydrol Earth Syst Sci*, 17(3), 1161–1175, doi:10.5194/hess-17-1161-2013, 2013.
- Alfieri, L., Feyen, L., Dottori, F. and Bianchi, A.: Ensemble flood risk assessment in Europe under high end climate scenarios, *Glob. Environ. Change*, 35, 199–212, doi:10.1016/j.gloenvcha.2015.09.004, 2015.
- Alfieri, L., Bisselink, B., Dottori, F., Naumann, G., de Roo, A., Salamon, P., Wyser, K. and Feyen, L.: Global projections of river flood risk in a warmer world, *Earths Future*, 2016EF000485, doi:10.1002/2016EF000485, 2016a.
- Alfieri, L., Feyen, L. and Baldassarre, G. D.: Increasing flood risk under climate change: a pan-European assessment of the benefits of four adaptation strategies, *Clim. Change*, 136(3), 507–521, doi:10.1007/s10584-016-1641-1, 2016b.
- Apel, H.; Thielen, A.H.; Merz, B.; Blöschl, G. Flood risk assessment and associated uncertainty. *Nat. Hazards Earth Syst. Sci.* 4, 295–308, 2004
- Arnell, N. W. and Gosling, S. N.: The impacts of climate change on river flood risk at the global scale, *Clim. Change*, 1–15, doi:10.1007/s10584-014-1084-5, 2014.
- Bachmair, S., Stahl, K., Collins, K., Hannaford, J., Acreman, M., Svoboda, M., ... & Crossman, N. D. Drought indicators revisited: the need for a wider consideration of environment and society. *Wiley Interdisciplinary Reviews: Water*, 2016.
- Bernie, D., and Lowe J. Future temperature responses based on IPCC and other existing emissions scenarios. AVOID2 WPA.1 Report 1, 2014 Available at www.avoid.uk.net
- Blauhut, V., Gudmundsson, L., & Stahl, K. Towards pan-European drought risk maps: quantifying the link between drought indices and reported drought impacts. *Environmental Research Letters*, 10(1), 014008. doi:10.1088/1748-9326/10/1/014008, 2015.
- Blauhut, V., Stahl, K., Stagge, J. H., Tallaksen, L. M., De Stefano, L., and Vogt, J. Estimating drought risk across Europe from reported drought impacts, drought indices, and vulnerability factors, *Hydrol. Earth Syst. Sci.*, 20, 2779-2800, 2016.
- Bontemps, S., Defourny, P., Bogaert, E. V., Arino, O., Kalogirou, V. and Perez, J. R.: GLOBCOVER 2009-Products description and validation report, [online] Available from: <http://www.citeulike.org/group/15400/article/12770349> (Accessed 9 August 2016), 2011.
- Boone, A. and P. Etchevers. "An intercomparison of three snow schemes of varying complexity coupled to the same land surface model: Local-scale evaluation at an Alpine site." *Journal of Hydrometeorology* 2(4): 374-394, 2001.
- Brooks N. Vulnerability, risk and adaptation: a conceptual framework Tyndall Centre for Climate Change Research Working Paper, 38 pp 1–16, 2003.
- Burek, P., Knijff van der, J. and Roo de, A. LISFLOOD, distributed water balance and flood simulation model revised user manual 2013., Publications Office, Luxembourg. Available online from: <http://dx.publications.europa.eu/10.2788/24719> (Accessed 12 December 2014a), 2013.
- Carpenter, T. M., Sperflage, J. A., Georgakakos, K. P., Sweeney, T. and Fread, D. L.: National threshold runoff estimation utilizing GIS in support of operational flash flood warning systems, *J. Hydrol.*, 224(1–2), 21–44, 1999.
- Carrão, H., Naumann, G., Barbosa, P. Mapping global patterns of drought risk: An empirical framework based on sub-national estimates of hazard, exposure and vulnerability. *Global Environmental Change*, 39, 108-124, 2016.
- Ciais, P., M. Reichstein, N. Viovy, A. Granier, J. Ogée, V. Allard, M. Aubinet, N. Buchmann, C. Bernhofer and A. Carrara. "Europe-wide reduction in primary productivity caused by the heat and drought in 2003." *Nature* 437(7058): 529-533, 2005.
- d'Orgeval, T. Impact du changement climatique sur le cycle de l'eau en Afrique de l'Ouest: modélisation et incertitudes, Université Paris VI: 188, 2006.
- d'Orgeval, T., Polcher, J. and de Rosnay, P. Sensitivity of the West African hydrological cycle in ORCHIDEE to infiltration processes, *Hydrol. Earth Syst. Sci.*, 12(6), 1387–1401, doi:10.5194/hessd-5-2251-2008, 2008.
- de Groeve T, Poljansek K, Ehrlich D and Corbane C. Current status and best practices for disaster loss data recording in EU member states EUR—Scientific and Technical Research Series p 162, 2014.
- de Rosnay, P., Polcher, J., Bruen, M. and Laval, K. Impact of a physically-based soil water flow and soil-plant interaction representation for modeling large-scale land surface processes, *J. Geophys. Res.*, 107(2), ACL 3 1–18, doi:10.1029/2001JD000634, 2002.

- Di Baldassarre, G., Viglione, A., Carr, G., Kuil, L., Salinas, J. L. and Blöschl, G.: Socio-hydrology: Conceptualising human-flood interactions, *Hydrol. Earth Syst. Sci.*, 17(8), 3295–3303, doi:10.5194/hess-17-3295-2013, 2013.
- Dottori, F., Salamon, P., Bianchi, A., Alfieri, L., Hirpa, F. A. and Feyen, L.: Development and evaluation of a framework for global flood hazard mapping, *Adv. Water Resour.*, 94, 87–102, doi:10.1016/j.advwatres.2016.05.002, 2016.
- Ducoudré, N.I., Laval, K. and Perrier, A. SECHIBA, a new set of parameterizations of the hydrologic exchanges at the land-atmosphere interface within the LMD atmospheric general circulation model. *Journal of Climate*, 6(2), pp.248-273, 1993.
- ECLAC (Economic Commission for Latin America and the Caribbean). *Handbook for Estimating the Socio-Economic and Environmental Effects of Disasters* (Mexico: ECLAC World Bank), 2003.
- Ehret, U., Zehe, E., Wulfmeyer, V., Warrach-Sagi, K. and Liebert, J.: HESS Opinions “Should we apply bias correction to global and regional climate model data?,” *Hydrol Earth Syst Sci*, 16(9), 3391–3404, doi:10.5194/hess-16-3391-2012, 2012.
- Elith, J. et al. A statistical explanation of MaxEnt for ecologists. *Div. Distrib.* 17, 43-57, 2010.
- Forzieri, G., Feyen, L., Russo, S., Voudoukas, M., Alfieri, L., Outten, S., Migliavacca M, Bianchi A, Rojas R, Cid, A. Multi-hazard assessment in Europe under climate change. *Climatic Change*, 1-15, 2016.
- Freire, S., Kemper, T., Pesaresi, M., Florczyk, A. and Syrris, V.: Combining GHSL and GPW to improve global population mapping, vol. 2015–November, pp. 2541–2543, 2015.
- Friedlingstein, P. et al. Climate-carbon cycle feedback analysis: Results from the C4MIP model intercomparison. *Journal of Climate*, 19, 3337-3353, 2006.
- GISTEMP Team: GISS Surface Temperature Analysis (GISTEMP). [online] Available from: <http://data.giss.nasa.gov/gistemp/> (Accessed 27 September 2016), 2016.
- Godfray, H.C.J., Beddington, J.R., Crute, I.R., Haddad, L., Lawrence, D., Muir, J.F., Pretty, J., Robinson, S., Thomas, S.M., Toulmin, C. Food Security: The Challenge of Feeding 9 Billion People. *Science* 327, 812. doi:10.1126/science.1185383, 2010.
- Gohar, L., S. Raper and J. Lowe. Reducing the uncertainty in simple model projections. *AVOID Report 25*, 2011.
- Guimberteau, M., Ducharne, A., Ciais, P., Boisier, J.P., Peng, S., De Weirtdt, M. and Verbeeck, H. Testing conceptual and physically based soil hydrology schemes against observations for the Amazon Basin. *Geoscientific Model Development*, 7, pp.1115-1136, 2014.
- Hazeleger, W., Wang, X., Severijns, C., Ștefănescu, S., Bintanja, R., Sterl, A., Wyser, K., Semmler, T., Yang, S., van, den H., van, N., van, der L. and van, der W.: EC-Earth V2.2: Description and validation of a new seamless earth system prediction model, *Clim. Dyn.*, 39(11), 2611–2629, doi:10.1007/s00382-011-1228-5, 2012.
- Hergarten S. Aspects of risk assessment in power-law distributed natural hazards *Nat. Hazards Earth Syst. Sci.* 4 309–13, 2004.
- Hirabayashi, Y., Mahendran, R., Koirala, S., Konoshima, L., Yamazaki, D., Watanabe, S., Kim, H. and Kanae, S.: Global flood risk under climate change, *Nat. Clim. Change*, 3(9), 816–821, doi:10.1038/nclimate1911, 2013.
- Hosking, J. R. M.: L-Moments: Analysis and Estimation of Distributions Using Linear Combinations of Order Statistics, *J. R. Stat. Soc. Ser. B Methodol.*, 52(1), 105–124, 1990.
- Huang, S., Krysanova, V. and Hattermann, F. F.: Does bias correction increase reliability of flood projections under climate change? A case study of large rivers in Germany, *Int. J. Climatol.*, 34(14), 3780–3800, doi:10.1002/joc.3945, 2014.
- Huizinga, H. J. and De Moel, H.: *Global Flood Damage Functions - Report Tasks 1&2: Review of existing data sources and Global flood damage functions database*, HKV Lijn in water, Lelystad, the Netherlands, 2016.
- IPCC 2007a. *Climate change 2007: The physical science basis. Contribution of Working Group I to the Fourth Assessment Report of the Intergovernmental Panel on Climate Change*. Cambridge University Press, Cambridge
- IPCC 2007b, *Climate Change 2007: Impacts, Adaptation and Vulnerability: Working Group II Contribution to the Fourth Assessment Report of the Intergovernmental Panel on Climate Change*, Cambridge University Press, 2007.
- IPCC 2012, *Managing the risks of extreme events and disasters to advance climate change adaptation. A Special Report of Working Groups I and II of the Intergovernmental Panel on Climate Change*, Cambridge University Press, 2012.
- IPCC 2013. *Climate Change 2013: The Physical Science Basis. Contribution of Working Group I to the Fifth Assessment Report of the Intergovernmental Panel on Climate Change* [Stocker, T.F., Qin, G.-K., Plattner, M., Tignor, S.K., Allen, J., Boschung, J., Naueis, A., Xia, Y., Bex V., and Midgley P.M. (eds).] Cambridge University Press, Cambridge, UK and New York, NY, USA, 1535 pp, Cambridge University Press, 2013.
- James, R. and Washington, R.: Changes in African temperature and precipitation associated with degrees of global warming, *Clim. Change*, 117(4), 859–872, doi:10.1007/s10584-012-0581-7, 2013.

- JMA: Global Warming Projection and Climate Change Monitoring, Tokyo Climate Center, Climate Prediction Division, Japan Meteorological Agency; <http://ds.data.jma.go.jp/tcc/tcc/products/gwp/gwp.html>, 2016.
- Jongman, B., Ward, P. J. and Aerts, J. C. J. H.: Global exposure to river and coastal flooding: Long term trends and changes, *Glob. Environ. Change*, 22(4), 823–835, doi:10.1016/j.gloenvcha.2012.07.004, 2012.
- Jongman, B., Hochrainer-Stigler, S., Feyen, L., Aerts, J. C. J. H., Mechler, R., Botzen, W. J. W., Bouwer, L. M., Pflug, G., Rojas, R. and Ward, P. J.: Increasing stress on disaster-risk finance due to large floods, *Nat. Clim. Change*, 4(4), 264–268, doi:10.1038/nclimate2124, 2014.
- Jonkman, S. N.: Global perspectives on loss of human life caused by floods, *Nat. Hazards*, 34(2), 151–175, doi:10.1007/s11069-004-8891-3, 2005.
- Kendall, M. G.: Rank Correlation Methods, 4th edition., Charles Griffin, London., 1975.
- Kostyack, J., *et al.* Beyond reserves and corridors: Policy solutions to facilitate the movement of plants and animals in a changing climate. *BioScience*, 61 (9): 713-719, 2011.
- Koutroulis, A. G., Grillakis, M. G., Daliakopoulos, I. N., Tsanis, I. K. and Jacob, D.: Cross sectoral impacts on water availability at +2 °C and +3 °C for east Mediterranean island states: The case of Crete, *J. Hydrol.*, 532, 16–28, doi:10.1016/j.jhydrol.2015.11.015, 2016.
- Kreibich, H. and Thielen, A. H.: Coping with floods in the city of Dresden, Germany, *Nat. Hazards*, 51(3), 423–436, doi:10.1007/s11069-007-9200-8, 2009.
- Krinner, G., Viovy, N., de Noblet-Ducoudré, N., Ogée, J., Polcher, J., Friedlingstein, P., Ciais, P., Sitch, S. and Prentice, I.C. A dynamic global vegetation model for studies of the coupled atmosphere-biosphere system. *Global Biogeochemical Cycles*, 19(1), 2005.
- Lobell, D.B., Burke, M.B., Tebaldi, C., Mastrandrea, M.D., Falcon, W.P., Naylor, R.L. Prioritizing Climate Change Adaptation Needs for Food Security in 2030. *Science* 319, 607–610. doi:10.1126/science.1152339, 2008.
- Lobell, D.B., Schlenker, W., Costa-Roberts, J. Climate Trends and Global Crop Production Since 1980. *Science* 333, 616–620. doi:10.1126/science.1204531, 2011.
- Mann, H. B.: Non-parametric tests against trend, *Econometrica*, 13, 163–171, 1945.
- Maia R, Vivas E, Serralheiro R and de Carvalho M. Socioeconomic evaluation of drought effects *Water Resour. Manage.* 29 575–88, 2014.
- Mastrandrea, M. D., Field, C. B., Stocker, T. F., Edenhofer, O., Ebi, K. L., Frame, D. J., Held, H., Kriegler, E., Mach, K. J., Matschoss, P. R., Plattner, G.-K., Yohe, G. W. and Zwiers, F. W.: Guidance note for lead authors of the IPCC fifth assessment report on consistent treatment of uncertainties, Intergovernmental Panel on Climate Change, Geneva Switzerland, 4 pp., 2010.
- Merz B, Elmer F and Thielen AH. Significance of ‘high probability/low damage’ versus ‘low probability/high damage’ flood events *Nat. Hazards Earth Syst. Sci.* 9 1033–46, 2009.
- Muerth, M. J., Gauvin St-Denis, B., Ricard, S., Velázquez, J. A., Schmid, J., Minville, M., Caya, D., Chaumont, D., Ludwig, R. and Turcotte, R.: On the need for bias correction in regional climate scenarios to assess climate change impacts on river runoff, *Hydrol. Earth Syst. Sci.*, 17(3), 1189–1204, doi:10.5194/hess-17-1189-2013, 2013.
- Munich Re: NatCatSERVICE - Loss events worldwide 1980 – 2014, Munich., 2015.
- Naumann G., Spinoni J., J. Vogt and P. Barbosa. Assessment of drought damages and their uncertainties in Europe. *Environmental Research Letters*, 10 124013. doi:10.1088/1748-9326/10/12/124013, 2015.
- Naumann G, Dutra E, Barbosa P, Pappenberger F, Wetterhall F, Vogt JV. Comparison of drought indicators derived from multiple data sets over Africa. *Hydrology and Earth System Sciences* 18: 1625-1640, 2014.
- Pesaresi, M., Huadong, G., Blaes, X., Ehrlich, D., Ferri, S., Gueguen, L., Halkia, M., Kauffmann, M., Kemper, T., Lu, L. and others: A global human settlement layer from optical HR/VHR RS data: concept and first results, *IEEE J. Sel. Top. Appl. Earth Obs. Remote Sens.*, 6(5), 2102–2131, 2013.
- Piao, S., Friedlingstein, P., Ciais, P., de Noblet-Ducoudré, N., Labat, D. and Zaehle, S. Changes in climate and land use have a larger direct impact than rising CO₂ on global river runoff trends. *Proceedings of the National academy of Sciences*, 104(39), pp.15242-15247, 2007.
- Rogel, J., M. Meinshausen, R. Knutti. Global warming under old and new scenarios using IPCC climate sensitivity range estimates. *Nature Climate Change* 2, 248–253, 2012.
- Root, T. L. and S. H. Schneider. Conservation and climate change: The challenges ahead. *Conservation Biology* 20 (3): 706-708, 2006.
- Sacks, W.J., Deryng, D., Foley, J.A., Ramankutty, N. Crop planting dates: an analysis of global patterns: *Global crop planting dates. Global Ecology and Biogeography* no-no. doi:10.1111/j.1466-8238.2010.00551.x, 2010.

- Sampson, C., Smith, A., Bates, P., Neal, J., Alfieri, L. and Freer, J. A high-resolution global flood hazard model, *Water Resour Res*, 51, 7358–7381, doi:10.1002/2015WR016954, 2015.
- Scussolini, P., Aerts, J. C. J. H., Jongman, B., Bouwer, L. M., Winsemius, H. C., de Moel, H. and Ward, P. J.: FLOPROS: an evolving global database of flood protection standards, *Nat Hazards Earth Syst Sci*, 16(5), 1049–1061, doi:10.5194/nhess-16-1049-2016, 2016.
- Smith K and Ward R. *Floods: Physical Processes and Human Impacts* (Chichester: Wiley), 1998.
- Swain, S., and Hayhoe, K. CMIP5 projected changes in spring and summer drought and wet conditions over North America. *Climate Dynamics*, 44(9-10), 2737-2750, 2015.
- Thiemeßl, M. J., Gobiet, A. and Heinrich, G.: Empirical-statistical downscaling and error correction of regional climate models and its impact on the climate change signal, *Clim. Change*, 112(2), 449–468, doi:10.1007/s10584-011-0224-4, 2012.
- Traore, A.K., Ciais, P., Vuichard, N., Poulter, B., Viovy, N., Guimberteau, M., Jung, M., Myneni, R. and Fisher, J.B. Evaluation of the ORCHIDEE ecosystem model over Africa against 25 years of satellite-based water and carbon measurements. *Journal of Geophysical Research: Biogeosciences*, 119(8), pp.1554-1575, 2014.
- UNDP (United Nations Development Programme), *Reducing Disaster Risk—A challenge for Development—A Global Report* New York, USA, 2004.
- UNFCCC: Paris Agreement, Conference of the Parties, Twenty-first session (COP21), Paris., 2015.
- UNISDR: Making development sustainable, the future of disaster risk management: Global assessment report on disaster risk reduction 2015, United Nations Office for Disaster Risk Reduction (UNISDR), Geneva, Switzerland. [online] Available from: <https://www.unisdr.org/we/inform/publications/42809> (Accessed 19 August 2016), 2015.
- UNISDR and CRED: The human cost of weather-related disasters 1995-2015, United Nations Office for Disaster Risk Reduction (UNISDR) and Centre for Research on the Epidemiology of Disasters (CRED), 2015.
- Urban, M.C. Accelerating extinction risk from climate change. *Science* 348 (6234): 571-573, 2015.
- van Vuuren DP, Lowe J, Stehfest E, Gohar L, Hof AF, Hope C, Warren R, Meinshausen M, Plattner GK. How well do integrated assessment models simulate climate change? *Climatic change* 104(2): 255-285, 2011.
- van der Knijff, J. M., Younis, J. and de Roo, A. P. J.: LISFLOOD: A GIS-based distributed model for river basin scale water balance and flood simulation, *Int J Geogr Inf Sci*, 24(2), 189–212, 2010.
- Veldkamp, T. I. E., Wada, Y., Aerts, J. C. J. H., Ward, P. J. Towards a global water scarcity risk assessment framework: incorporation of probability distributions and hydro-climatic variability. *Environmental Research Letters*, 11(2), 024006, 2016.
- Viovy, N. and de Noblet, N.: Coupling water and Carbon cycle in the biosphere, *Sci. Géol. Bull.*, 50, 109–121, 1997.
- Vogt JV and Somma F (eds): *Drought and Drought Mitigation in Europe* (Advances in Natural and Technological Hazards Research vol 14) (Dordrecht: Kluwer) pp 325, 2000.
- Wang, T., Ottlé, C., Boone, A., Ciais, P., Brun, E., Morin, S., Krinner, G., Piao, S. and Peng, S. Evaluation of an improved intermediate complexity snow scheme in the ORCHIDEE land surface model. *Journal of Geophysical Research: Atmospheres*, 118(12), pp.6064-6079, 2013.
- Ward, P. J., Jongman, B., Kumm, M., Dettinger, M. D., Weil, F. C. S. and Winsemius, H. C.: Strong influence of El Niño Southern Oscillation on flood risk around the world, *Proc. Natl. Acad. Sci. U. S. A.*, 111(44), 15659–15664, doi:10.1073/pnas.1409822111/-/DCSupplemental, 2014.
- Warren, R., J. VanDerWal, J. Price, J. Welbergen, I. Atkinson, J. Ramirez-Villegas, T.J. Osborn, A. Jarvis, L.P. Shoo, S.E. Williams and J. Lowe. Quantifying the benefit of early mitigation in avoiding biodiversity loss. *Nature Climate Change* 3: 678- 682. (doi:10.1038/nclimate1887), 2013.
- Wilhite DA. *Drought assessment, management and planning: theory and case studies*. Kluwer Academic Publishers, 293 pp., ISBN 0-7923-9337-6, 1993.
- Williams, J. W. & Jackson, S. T. Novel climates, no-analog communities, and ecological surprises. *Front Ecol Environ* 5, 475-482, 2007.
- Williams, J. W., *et al.* Projected distributions of novel and disappearing climates by 2100 AD. *Proceedings of the National Academy of Sciences* 104: 5738-5742, 2007.
- Williams, S. E., *et al.* Towards an integrated framework for assessing the vulnerability of species to climate change. *PLoS Biol* 6 (12): e325, 2008.
- Wind, H. G., Nierop, T. M., De Blois, C. J. and De Kok, J. L.: Analysis of flood damages from the 1993 and 1995 Meuse floods, *Water Resour. Res.*, 35(11), 3459–3465, doi:10.1029/1999WR900192, 1999.
- Winsemius, H. C., Van Beek, L. P. H., Jongman, B., Ward, P. J. and Bouwman, A.: A framework for global river flood risk assessments, *Hydrol Earth Syst Sci*, 17(5), 1871–1892, doi:10.5194/hess-17-1871-2013, 2013.



- Winsemius, H. C., Aerts, J. C. J. H., van Beek, L. P. H., Bierkens, M. F. P., Bouwman, A., Jongman, B., Kwadijk, J. C. J., Ligtvoet, W., Lucas, P. L., van Vuuren, D. P. and Ward, P. J.: Global drivers of future river flood risk, *Nat. Clim. Change*, 6(4), 381–385, doi:10.1038/nclimate2893, 2016.
- Woodward, M., Gouldby, B., Kapelan, Z., Khu, S.-T. and Townend, I.: Real Options in flood risk management decision making, *J. Flood Risk Manag.*, 4(4), 339–349, doi:10.1111/j.1753-318X.2011.01119.x, 2011.
- Zurich: Risk Nexus, Central European floods: a retrospective. [online] Available from: http://www.zurich.com/_/media/dbe/corporate/docs/whitepapers/risk-nexus-may-2014-central-european-floods-2013.pdf, 2014.
- Zuur, A.F., Ieno, E.N., Elphick, C.S. A protocol for data exploration to avoid common statistical problems. *Methods in Ecology and Evolution* 1, 3–14. doi:10.1111/j.2041-210X.2009.00001.x, 2010.